Supporting Information for

Structural Basis for Superoxide Activation of *Flavobacterium johnsoniae* Class I Ribonucleotide Reductase and for Radical Initiation by its Dimanganese Cofactor

Hannah R. Rose,[1,‡] Manas K. Ghosh,[1,‡] Ailiena O. Maggiolo,[1,2] Christopher J. Pollock,[1] Elizabeth J. Blaesi,[1] Viviane Hajj,[1,5] Yifeng Wei,[3,6] Lauren J. Rajakovich,[2] Wei-chen Chang,[1,7] Yilin Han,[2] Mariana Hajj,[1,8] Carsten Krebs,[1,2,*] Alexey Silakov,[1,*] Maria-Eirini Pandelia,[4,*] J. Martin Bollinger, Jr.,[1,2,*] and Amie K. Boal[1,2,*]

AFFILIATIONS:
[1]Department of Chemistry, The Pennsylvania State University, University Park, PA
[2]Department of Biochemistry and Molecular Biology, The Pennsylvania State University, University Park, PA
[3]Present address: Cornell High Energy Synchrotron Source, Cornell University, Ithaca, NY
[4]Department of Chemistry, Massachusetts Institute of Technology, Cambridge, MA 02139
[5]Present Address: Metabolic Engineering Research Laboratory, Singapore
[6]Present Address: Department of Chemistry, Harvard University, Cambridge, MA
[7]Present Address: Department of Chemistry, North Carolina State University, Raleigh, NC
[8]Present Address: Lebanese University, Faculty of Public Health, Saida, Lebanon
[9]Department of Biochemistry, Brandeis University, Waltham, MA
[‡]Equal contributions/co-first authors
*Authors to whom correspondence should be addressed: ckrebs@psu.edu; aus40@psu.edu; mepandelia@brandeis.edu; jmb21@psu.edu; akb20@psu.edu.

Materials. Yeast extract, dithiothreitol (DTT), isopropyl-β-D-thiogalactopyranoside (IPTG), Tris(hydroxymethyl)aminomethane (Tris) and kanamycin were purchased from DOT Scientific. Tryptone and ferrous ammonium sulfate hexahydrate [$Fe(NH_4)_2SO_4 \bullet 6H_2O$] were purchased from Fisher Scientific. Chloramphenicol was purchased from IBI Scientific. 4-(2-Hydroxyethyl)-1-piperazineethanesulfonic acid (HEPES) was purchased from Chem-Impex International. Glycerol was purchased from Macron Fine Chemicals. Phenylmethylsulfonyl fluoride (PMSF) was purchased from Amresco. Ammonium formate was purchased from Fluka. Streptomycin sulfate, formic acid, 1,4-dihydroxybenzene (hydroquinone, HQ), 1,4-dihydroxynaphthalene (naphthohydroquinone, NQ), riboflavin 5'-monophosphate (FMN), flavin adenine dinucleotide (FAD), disodium dithionite ($Na_2S_2O_4$), disodium adenosine-5'-triphosphate (ATP) hydrate, sodium cytidine-5'-diphosphate (CDP) hydrate, disodium ethylenediaminetetraacetic acid hydrate (EDTA), 1,10-phenanthroline, methyl viologen (1,1'-dimethyl-4,4'-bipyridinium dichloride), 2-mercaptoethanol, Sephadex G-50 resin, xanthine, xanthine oxidase, and cytochrome C were purchased from Sigma-Aldrich. Ferrozine [3-(2-pyridyl)-5,6-bis(4-phenylsulfonic acid)-1,2,4-triazine], magnesium sulfate ($MgSO_4$), manganous chloride ($MnCl_2$), and imidazole were purchased from Alfa Aesar. Ni^{II}-nitrilotriacetic acid agarose (Ni-NTA) resin was purchased from MCLAB. Nitric acid (HNO_3), sodium chloride (NaCl), sodium hydroxide (NaOH), calcium chloride ($CaCl_2$), ammonium chloride (NH_4Cl) and Amicon Ultra-15 centrifugal filters were purchased from EMD Millipore. Ammonium hydroxide (NH_4OH) and monobasic potassium phosphate (KH_2PO_4) were purchased from VWR International. Hydrogen peroxide (H_2O_2), glucose, sodium dodecyl sulfate (SDS) and dibasic sodium phosphate (Na_2HPO_4) were purchased from J. T. Baker. Oligonucleotide primers were purchased from Integrated DNA Technologies. Polymerase chain reaction (PCR) reagents, Phusion polymerase, restriction enzymes, restriction enzyme buffers, and T4 DNA ligase were purchased from New England Biolabs. The kit for extraction of DNA from agarose gels was purchased from Qiagen. *Escherichia coli* (*Ec*) BL21 (DE3) cells, Rosetta (DE3) cells, and the pET-28a(+) vector were purchased from Novagen. ^{57}Fe metal was purchased from Isoflex (San Francisco, CA). N_3-UDP (2'-azido-2'-deoxyuridine-5'-diphosphate) was a gift from by Prof. JoAnne Stubbe (Massachusetts Institute of

Technology). Genomic DNA from *Flavobacterium johnsoniae* (*Fj*) was a gift from Prof. Ryan Rhodes (University of North Carolina, Wilmington).

DNA Vectors for Over-expression of His_6-affinity-tagged Versions of α and β Subunits of Fj RNR in Ec. The vectors directing over-expression of the *Fj* class Id ribonucleotide reductase (RNR) α and β subunits were constructed by the following procedure. The coding sequences were amplified from *Fj* genomic DNA by PCR using Phusion polymerase (New England Biolabs) and the primers shown below (non-coding sequence is in lower case).

	Primer	Sequence
α	Forward	5'-ccgcgaacagattggaggtATGAATACAATAGATCCAAATGAAGTAAATAGTCTTCCGC-3'
	Reverse	5'-cgaattcggatcctctagtcaTCATGATTCACAGCTGCTGCAAGAAACAAGACTCG-3'
β	Forward	5'-ccgcgaacagattggaggtATGTCTATATTTGATAAAAGAGTCAATTATAAACC-3'
	Reverse	5'-cgaattcggatcctctagtcaTTAGAAAAGGTCGTTTGCCGTGATGCTTTTATCG-3'

The genes were inserted into a linearized pE-SUMO vector (Lifesensors) by Gibson assembly. The coding sequences were then re-amplified by PCR using the resultant vectors as templates and the primers shown below (restriction sites are shown in bold).

	Primer	Sequence
α	Forward	5'-ACTGTA**CATATG**AATACAATAGATCCAAATGAAGTAAATAGTCTTCCGCA-3'
	Reverse	5'-GTAGT**CTCGAG**TCATCATGATTCACAGCTGCTGCAAGAAAC-3'
β	Forward	5'-ACTGTA**CATATG**TCTATATTTGATAAAAGAGTCAATTATAAACCTTTTGAATACCCGGAG-3'
	Reverse	5'-GTAGT**CTCGAG**TCATCATGATTCACAGCTGCTGCAAGAAAC-3'

The amplicons were purified by gel electrophoresis and re-isolated by using the Qiagen gel extraction kit. The amplicons were ligated with the pET-28a(+) vector at the *Nde*I and *Xho*I restriction sites (Life Technologies). This gene construct encodes an N-terminal His_6 tag with a full amino acid sequence of $MGS_2H_6S_2GLVPRGSH$. The ligation reaction was used to transform BL21(DE3) cells and successful transformants were selected on kanamycin-supplemented (50 μg/ml) LB agar plates. The DNA sequences of

the entire coding regions of both expression vectors (found in SI) were verified by dnaTools, Inc.

Construction of Vector for Overexpressing Y104F variant of Fj β. The Tyr 104→Phe substitution was introduced into the *Fj* RNR β protein by modifying the encoding vector using the Stratagene QuikChange II kit according to the manufacturer's instructions. The pET28a-*Fj* β wt was used as the template and the following mutagenic primers encoding the desired substitution were used: Forward: 5'-CAG ACA TTC TGA AGC GTT TTC TCG TCT TTT GGA AG-3' and Reverse: 5'-CTT CCA AAA GAC GAG AAA ACG CTT CAG AAT GTC TG-3'. The sequences of the coding regions (below) were verified by dnaTools, Inc.

α subunit:

ATGGGCAGCAGCCATCATCATCATCATCACAGCAGCGGCCTGGTGCCGCGCG
GCAGCCATATGAATACAATAGATCCAAATGAAGTAAATAGTCTTCCGCATAA
TGAAGCAGGAACCAAAATGTGGTGGAAGAACTCTGAAAGTGAACAAATTTTA
AATCGTGGTTATCTTTTAAAAGGAGAAACAGTAGAAGGTGCAATTGACAGAA
TTTGTACGGCTGCTGCCAGAAGATTATACAAACCAGAATTAAAAGAGTCTTTT
GTAGAAATGATCGAACGCGGCTGGATGAGTATCAGTTCGCCGGTCTGGGCTA
ATATGGGAACCGAAAGAGGTCTGCCTATTTCTTGTTTTAACGTTCACGTTCCG
GATAAAATTGAAGGAATTACACATAAATTAGGCGAAGTAATCATGCAGACTA
AAATAGGTGGTGGAACATCTGGTTATTTTGGAGAATTGCGTGAGCGCGGAAG
TGCCGTAACCGATAACGGAAAAAGCAGCGGTGCCGTAAGTTTTATGAAACTT
TTTGATACGGCTATGGATACGATTTCGCAAGGCGGAGTACGCCGCGGTGCAT
TTGCAGCGTATTTGGATATTGACCATCCGGATATCGAGGAGTTTTTGAAAATT
AAAAGTATTGGAAATCCAATTCAGAATTTATTTACCGGAATCTGTGTGCCGG
ATTACTGGATGCAGGAAATGATTGATGGTGATGCTGATAAAAGACAAATTTG
GGCAAAAGTATTAGAAAGCCGTCAGCAGAAAGGACTGCCGTATATCTTTTTC
AGCGATAACGTAAATAAAAACAAACCACAGGTTTATAAAGATCAAAACCTA
AGAATCAATGCAAGTAATTTATGCAGTGAGATTATGCTTCCGTCAACTCATGA
CGAATCATTTATCTGCTGTCTTTCTTCTATGAACTTAGAATTGTATGAAGAAT

GGAAAGATACTGAAGCGGTAAAACTGGCGATCTTTTTCTTAGATGCAGTTTTA
CAGGAATTCATCGAAAAAACAGAAGGCAACTATTATCTTTCTGCAGCAAATA
AATTTGCTAAAAGACACCGTGCGCTTGGATTAGGTGTTTTAGGATGGCATTCT
TATCTGCAAAAAAATATGATTCCGTTTGAAGGAATGGAAGCTAAAATGAAAA
CAACAGAGATTTTCAAACATATAAGTGATAAAGCGGATAAAGCAAGTCAGG
AACTGGCTAGAATTTACGGTGAACCAGAATTGTTAAAAGGTTACGGAAGACG
TAATACCACTACAATGGCAATTGCTCCAACGACTTCATCTTCTGCTATTTTAG
GACAGACTTCACCAGGAATTGAACCTTTCAGCAGTAATTATTATAAAGCTGG
ATTAAGCAAAGGTAATTTCATGCGTAAGAATAAATATCTTAAAAAGTTATTA
GAAGAAAAAGGTTTAGACAATGAAGAAGTCTGGAGAGGAATTATGCTAAAC
GGAGGAAGCGTTCAGCACATGTCACAACTAACACAGCAGGAAAAAGATGTTT
TTAAAACATTTAAAGAAATCAGCCAGTTAGAAATTGTTCAACAGGCAGGAAT
TCGTCAGAAATTTGTAGATCAGGGACAAAGTTTAAATCTTAATATTCCGGCTG
AATTAGCGATTAAAGATGTAAACCGTTTAATGATCGAAGCCTGGCAGCAAGG
AGTTAAAAGTTTGTACTACCAAAGAAGCCAGAGTGTTTCTAAAGAATTAGTA
ACGAGTCTTGTTTCTTGCAGCAGCTGTGAATCA.

<u>β subunit</u>:

ATGGGCAGCAGCCATCATCATCATCATCACAGCAGCGGCCTGGTGCCGCGCG
GCAGCCATATGTCTATATTTGATAAAAGAGTCAATTATAAACCTTTTGAATAC
CCGGAGGTTTTACAATTTACAGAAGCGATAAATAAAGCGTATTGGGTTCATA
CAGAAGTTGATTTTACTGCTGATACTCAGGATTTTCACGCTCACTTATCTCTG
GCAGAGAAAACAGCGGTAAAAAACAGTCTGCTGGCAATTGCACAGATTGAG
GTAGCCGTAAAAAGTTTTTGGGGAAACATTTACGAGCATTTTCCAAAACCAG
AATTTAATGGTTTAGGAAGTACTTTTGCTGAGTGTGAATTCAGACATTCTGAA
GCGTATTCTCGTCTTTTGGAAGTGTTAGGTTATAATGATGAATTTGAAAAACT
TCTGGATGTACCAGTTATTCGTCGTCGTGTAGATTACCTTTCAAATGTACTTA
AAGATACCAAATCTCAGGACAACAGAAAATATATGGTTTCGCTGATCTTATT
CAGTATTCTGATCGAAAATGTTTCGCTTTTCAGCCAGTTTGCCATCTTGCTTTC
TTTTACAAGATTTAAGGGGTACATGAAAAATGTGAGCAACATTATCGCCTGG
ACTTCTATTGATGAGCAGATTCATGCAAATGGAGGAATCTATATTATCAATAA

AATCAGAGAAGAATTCCCAGATTATTTTGATGAAGAAACTTTGGCTTTGGTG
AGAGAAACAGTTAAAGATTCTATTGCAGTCGAATCAGACATATTAGACTGGA
TATTTGAAGAAGGTGAAATTGAAAGTATTAAAAAAGGTGATTTAGTGAATTT
TATGAAATTTAGAATTGACGAAAGCCTGAAACAAATTAATATTCCGGTAATT
TTTGATGTAAAGGTTGAAGATTACAAAGCTCTGGCTTGGTTTGAAGAAGAAG
TTTTTGCCAACAGTCTGGACGATTTCTTTGCAAAACGCCCTGTAGAATACACT
AAACACGATAAAAGCATCACGGCAAACGACCTTTTC.

Details of LC-MS Method used to quantify product formation in RNR activity assays: The substrate CDP (*m/z* = 402) and product dCDP (*m/z* = 386) were eluted with a gradient of 25 mM ammonium formate at pH 9 (mobile phase A) and acetonitrile (mobile phase B). The elution gradient was: (1) 10 % B for 3 min; (2) 10 - 50 % B over 3 min; (3) 50 % B for 3 min; and (4) 50 - 10 % B over 7 min. Both CDP and dCDP were detected and quantified by mass spectrometry with electrospray ionization in the negative ion mode. The ratio of the area of the CDP or dCDP peak to the sum of the peak areas was multiplied by the initial concentration of CDP (2 mM) to obtain the concentrations of CDP and dCDP at each reaction time.[1]

Over-expression and Purification of Iron-dependent Superoxide Dismutase from Vigna unguiculata (Vu SOD). A pET-28a(+)-derived plasmid encoding N-terminally His_6-tagged iron-dependent *Vu* SOD[2] was kindly provided as a gift by José Fernando Morán (Universidad Publica de Navarra). The plasmid was used to transform *Ec* BL21(DE3) cells, which were grown and harvested as described above for expression of the *Fj* RNR β protein. Purification of the *Vu* SOD was carried as described for *Fj* β and yielded ~ 100 mg/L culture medium. The activity of the recombinant *Vu* SOD was verified by a published assay based on inhibition of O_2^--mediated cytochrome c reduction. This reduction occurs as xanthine oxidase produces O_2^- in the presence of xanthine and is inhibited in the presence of an active SOD.[3] The concentrations of *Vu* SOD reported are of its iron cofactor, determined by using a published colorimetric assay based on formation of the Fe^{II}-(ferrozine)$_3$ complex ($\varepsilon_{562} = 27{,}900\ M^{-1}cm^{-1}$).[4]

Over-expression and Purification of RNR β (NrdF) from Bacillus subtilis (Bs NrdF). A pET14b-derived vector encoding a His_6-affinity-tagged version of the *Bs* RNR β subunit (NrdF) was a kind gift from Prof. JoAnne Stubbe (Massachusetts Institute of Technology). Cell growth and protein over-production were carried out as previously described,[5] with one minor modification: 30 min before induction of expression, cultures were supplemented with 100 μM 1,10-phenanthroline to inhibit incorporation of iron into the protein. Approximately 20 g of cell paste was resuspended in 50 mM Tris-chloride, 5% glycerol (pH 7.6) supplemented with 1 mM PMSF and lysed via passage through a microfluidizer operating at 17,500 psi for 5 min. Centrifugation at 22,000*g* pelleted cell debris, and the supernatant was treated by the slow addition of a solution of 6% streptomycin sulfate to a final concentration of 1%. The solution was stirred for 15 min and then centrifuged. The clarified cell lysate was applied to a Ni-NTA column (25 mL) in the same buffer. The column was washed with four column volumes of buffer supplemented with 10 mM imidazole, after which buffer supplemented with 250 mM imidazole was applied. Fractions were collected and those containing NrdF (identified by SDS-PAGE) were combined and buffer exchanged via spin-concentration/redilution in a YM10 concentrator until the final concentration of imidazole was < 200 μM. Analysis of the resultant protein product by ICP-AES confirmed that the protein is in the apo form. Protein concentration was determined spectrophotometrically using the computationally derived extinction coefficient of 54,800 $M^{-1}cm^{-1}$ for the *Bs* β monomer (NrdF).

Over-expression and Purification of NrdI from Bacillus subtilis (Bs NrdI). A pET14b-derived vector encoding a His_6-affinity-tagged verson of the *Bs* NrdI protein (the flavoprotein activator of NrdF) was a kind gift from Prof. JoAnne Stubbe (Massachusetts Institute of Technology). Gene expression and purification of the NrdI were carried out as previously reported for the recombinant *E. coli* ortholog,[5] with the minor modifications described below. A greater mass of cells was utilized (~ 60 g), and so the sizes of the Ni-NTA and DEAE columns utilized were also increased accordingly. After frozen cell paste was resuspended, 1 mM PMSF was added. Cells were lysed by a 5 min passage through a microfluidizer operating at ~ 17,500 psi. After centrifugation to pellet the cell

debris, the clarified cell lysate was immediately applied to a Ni-NTA column in 50 mM sodium phosphate, 10% glycerol, pH 7.6. Elution of the NrdI protein, subsequent application to a DEAE column (GE Healthcare), and concentration of the pure protein product were all conducted as previously described.[5] The concentrations of *Bs* NrdI cited herein are of the flavin-bound protein, determined by using the published molar absorption coefficient (ε_{449}) of 9600 $M^{-1}cm^{-1}$.[5]

Production of activated Fj β for XAS and Titrations: N-terminally $(His)_6$-tagged *Fj* β protein was over-expressed in rich LB medium (procedure ***1***, in the presence of 5 mM 1,10-phenanthroline) and isolated as described, except that the lysis step was performed by sonication (QSonica Q500, 5 min total pulse time, 8 s on/30 s off, 50% amplitude) of re-suspended cells kept on ice. The protein was purified by Ni^{II}-NTA affinity chromatography, and imidazole was removed by gel filtration chromatography on a Superdex 200 column (GE Healthcare) by isocratic elution in 50 mM sodium HEPES, pH 7.6, 200 mM NaCl. For XAS sample preparation, concentrated β was diluted to 0.3 mM in assay buffer and activated by addition of 1-1.5 equiv Mn followed by 1 equiv NQ. Sub-stoichiometric amounts of Mn^{II} were added to ensure that all added Mn was bound to the protein and there was no free Mn^{II} in solution. The total reaction volume of the activation mixture was 8 mL of 0.3 mM β. Prior to addition of NQ, a small portion was removed to use as a Mn^{II} control. Following removal of NQ, the sample was concentrated to 2.3 mM β for XAS. 250 μL aliquots were loaded into Mössbauer cells sealed with 38 μm Kapton tape, which were then frozen in liquid N_2.

Production of the di-manganese Bs β (NrdF) cofactor. Solutions of NrdI and NrdF were rendered anoxic and brought into an anoxic chamber. Solutions of $MnCl_2$ (33 mM) and sodium dithionite (100 mM) were prepared in the box. Manganese was added to the NrdF protein to 2 equiv, and the solution was incubated at room temperature for ~ 5 min. Concurrently, NrdI was reduced via addition of 2 equiv dithionite. The reduced NrdI and Mn^{II}-loaded NrdF proteins were then mixed in a 2:1 molar ratio, the solution was incubated for ~ 5 min, and oxygen-saturated water was then rapidly added, thus introducing a large (> 50-fold) excess of O_2 over the NrdF protein. The resultant solution

was concentrated to < 2 mL and passed over an S200 size-exclusion column (HiLoad 16/600 Superdex 200 pg, GE Healthcare) to separate the NrdI and NrdF proteins. Fractions containing NrdF were concentrated to 2 mM monomer for analysis by XAS, and a diluted sample of this pool was used for analysis by EPR spectroscopy. Near-complete oxidation (> 90%) of the manganese present (to either the met or active cofactor state) was confirmed by the EPR analysis.

EPR and activity measurements of selected points in titration. The samples in Fig. S10 contain 0.3 mM β, 12 μM methyl viologen, and 0-1.5 equiv dithionite relative to Mn_2 (0-3 e^-/Mn_2). After measuring the UV-visible absorption spectrum, aliquots were removed for activity measurements and the remainder of the sample was transferred to a quartz EPR tube and frozen for EPR analysis. EPR spectra were measured at 10 K and 30 K, as described in the main text. Activity was measured at 21 ± 2 °C in the absence of O_2 with 40 μM *Vu* SOD included to prevent reoxidation of the cofactor.

Structure of Metal-stripped Fj Mn^{II}-β Crystallized Under Aerobic Conditions. N-terminally $(His)_6$-tagged *Fj* β protein was overexpressed in LB medium and isolated as described (procedure ***2***), except that the lysis step was performed by sonication (QSonica Q500, 5 min total pulse time, 8 s on/30 s off, 50% amplitude) of re-suspended cells kept on ice. The protein was purified by Ni^{II}-NTA affinity chromatography (as described above) and dialyzed into 50 mM sodium HEPES, pH 7.6, 50 mM NaCl (buffer A) for an additional anion exchange chromatography step (DEAE Sepharose, GE Healthcare). *Fj* β was eluted from the column at 350 mM NaCl when a gradient of 50 mM - 2 M NaCl (in 50 mM sodium HEPES, pH 7.6) was applied over 15 column volumes. The purified protein was dialyzed overnight at 4 °C against buffer A containing 10 mM EDTA to remove adventitiously bound metal ions. The EDTA was removed from the protein by gel filtration chromatography on a Superdex 200 column (GE Healthcare) by isocratic elution in 50 mM sodium HEPES, pH 7.6, 200 mM NaCl. EDTA-stripped *Fj* β was concentrated to 10 mg/mL in an Amicon Ultra 10-kDa MWCO centrifugal filter device and exchanged into 50 mM sodium HEPES, pH 7.6, 50 mM NaCl for crystallization trials. The protein was loaded with excess $MnCl_2$ (4/β) prior to crystallization by the

hanging drop vapor diffusion method at room temperature with 0.2 M magnesium acetate and 20% (w/v) PEG 3350 as the precipitating solution. The trials yielded several crystal morphologies. One of these, a set of triangular prism-shaped crystals, appeared within 1-2 days and diffracted x-rays to high resolution. The samples used for data collection were harvested from drops that were seeded with microcrystals obtained from identical crystallization conditions. The crystals were soaked briefly in a cryoprotectant solution [30% (v/v) glycerol, 0.2 M magnesium acetate, 20% (w/v) PEG 3350], harvested in rayon loops, and flash-frozen in liquid N_2. Phases were obtained by molecular replacement with Balbes[6], using the coordinates of *Bacillus halodurans* RNR β (PDB accession code 2RCC) as the initial search model. Data collection and refinement statistics are given in Table S5. The resulting model of *Fj* β was used to phase all subsequent datasets.

The final structural model consists of residues 1-300 for chain A, residues 1-300 for chain B, four Mn^{II} ions, two Mg^{II} ions and 109 water molecules (PDB accession code 6CWO). Electron density was not observed for any of the residues associated with the N-terminal tag or linker in chain A, but the six residues that immediately precede the N-terminal methionine of *Fj* β can be modeled in chain B (Figs. S25, S26). Continuous electron density was not observed for the final 24 residues at the C-terminus of the protein in either chain. However, a small portion of the C-terminus of chain A (residues 304-9) could be modeled as forming a crystallographic contact (Fig. S25) with the N-terminal region of a neighboring monomer. Although likely a crystallographic artifact, clear electron density exists for Tyr 311, the subunit-interfacial member of the radical-translocation pathway, for which no density has been observed in any other structure of a class I β.[7] Of the residues modeled, 97.4% are in allowed or preferred regions indicated by the Ramachandran statistical analysis.

Structure of Metal-stripped Fj Mn^{II}–β to Mn^{II} Crystallized Under Anaerobic Conditions.

A sample of the His_6-affinity-tagged *Fj* β (10 mg/mL in 50 mM sodium HEPES pH 7.6, 50 mM NaCl), obtained as described above, was purified as for the above sample but with phenanthroline included during cell growth (procedure ***1***). No additional metal chelation by EDTA or ferrozine was performed during the purification procedure.

Over-expression and Purification of N-terminally Strep-tagged Fj β. The sequence encoding *Fj* β was amplified from *Fj* genomic DNA by standard recombinant DNA methods using the primers shown below with restriction sites for *Bsa*I (underlined). Primer 1: 5'—CCG AGC **GGT CTC** GGC GCC ATG TCT ATA TTT GAT AAA AGA GTC A-A TTA TAA ACC TTT TG – 3' and primer 2: 5' – CCG AGC **GGT CTC** GTA TCA TTA GAA AAG GTC GTT TGC CGT GA – 3'

After restriction with *Bsa*I, the amplicon was ligated with pPR-IBA2 (IBA GmbH) using T4 DNA ligase. DH5α *Ec* cells were transformed with the ligation mixture, and plasmids from transformants (designated *Fj* β/pPR-IBA2) were verified by Sanger sequencing (Genomics Core Facility at Penn State University). BL21(DE3+) cells were transformed with *Fj* β/pPR-IBA2 and successful transformants were selected on LB agar plates containing 100 μg/mL ampicillin. Cultures (1 L) were following growth procedure **3,** except that cultures were supplemented with 100 μg/mL ampicillin. A typical yield of wet cell mass was ~3 g/L. To purify, cell paste (~12 g) was resuspended in 60 mL buffer (50 mM sodium HEPES, 300 mM NaCl, pH 8.0) with 0.1 mM PMSF and 0.5 mg/mL lysozyme and lysed via sonication (5 min total pulse time, 10 s on/30 s off, 60% amplitude). Cell debris was removed by centrifugation at 22,000*g*, and the supernatant was loaded onto a 10 mL TricornTM 10/100 column (GE Healthcare) packed with Strep-Tactin Superflow Plus resin (Qiagen). The column was washed with 5 column volumes of 50 mM sodium HEPES, 300 mM NaCl pH 8.0, and the protein was eluted with a linear gradient of 0-2.5 mM desthiobiotin over 15 column volumes. The fractions containing *Fj* β (determined by SDS-PAGE) were pooled, concentrated in an Amicon Ultra 10-kDa MWCO centrifugal filter device (Millipore) to ~2 mL, and loaded onto a Sup200 gel filtration column (GE Healthcare). The protein was eluted isocratically in 50 mM sodium HEPES, pH 7.6, 300 mM NaCl, 5% glycerol, frozen in liquid N_2, and stored at -80 °C.

Structure of As-Isolated Strep-tagged Fj β. As-isolated Strep-tagged *Fj* β [25 mg/mL in 50 mM HEPES pH 7.6, 150 mM NaCl, 5% (v/v) glycerol] was co-crystallized with excess (4 Mn/β) $MnCl_2$. Flat, rectangular-shaped crystals were obtained by the sitting-drop vapor-diffusion method at 4 °C with 20% (w/v) PEG 3350 and 0.1 M magnesium

formate as the precipitant. After mounting on rayon loops, crystals were soaked in cryoprotectant solution [20% (w/v) PEG 3350, 0.1 M magnesium formate, 30% glycerol] for less than 5 min and flash-frozen in liquid N_2.

The structure was solved using the coordinates of metal-stripped *Fj* β co-crystallized with Mn^{II} as the initial search model (Table S6). The final model consists of residues 1-306 for chain A, residues 1-300 for chain B, 4 Mn^{II} ions, 162 water molecules, and 2 Mg^{II} ions (PDB accession code 6CWQ). At the N-terminus, the GA linker residues of the strep tag were modeled (Fig. S26), but insufficient density for the final 18 (chain A) or 24 (chain B) residues was observed. Ramachandran plots indicate that 100% of the residues are in allowed or preferred regions. Anomalous difference Fourier maps collected at the Mn^{II} absorption edge reveal strong density at both Mn^{II} sites (Fig. S27), with occupancies between 0.85-0.95. A dataset for the same protein crystallized without additional Mn^{II} was also collected (not shown), and it displayed similar metal ion occupancy levels.

Analysis of cavities and channels in x-ray structures. Cavities were mapped using the program HOLLOW[8] with volume calculations performed using the DoGSiteScorer server.[9]

Sequence Similarity Networks (SSN). All searches were carried out using, and sequences and taxonomic information were retrieved from, the National Center for Biotechnology Information (NCBI) and PubMed databases, unless stated otherwise. The sequences that were used for the construction of the SSNs were retrieved from the InterPro Database (IPR000358) and belong to the ribonucleotide reductase small subunit superfamily (12,348 sequences as of December 2015). The SSNs were generated using the internet-based Enzyme Function Initiative Enzyme Similarity Tool (EFI-EST) (http://efi.igb.illinois.edu/efi-est/).[10] As input, the user-specified IPR000358 family was combined with a manually curated FASTA file containing the 157 sequences included in the phylogenetic analysis (*vide infra*). This approach allows for full contextualization, within the entire IPR000358 family, of the subset of sequences used to infer phylogenetic relationships. Figures that illustrate SSN analyses were created in Cytoscape (v3.1.1).

Supplementary Figures and Schemes

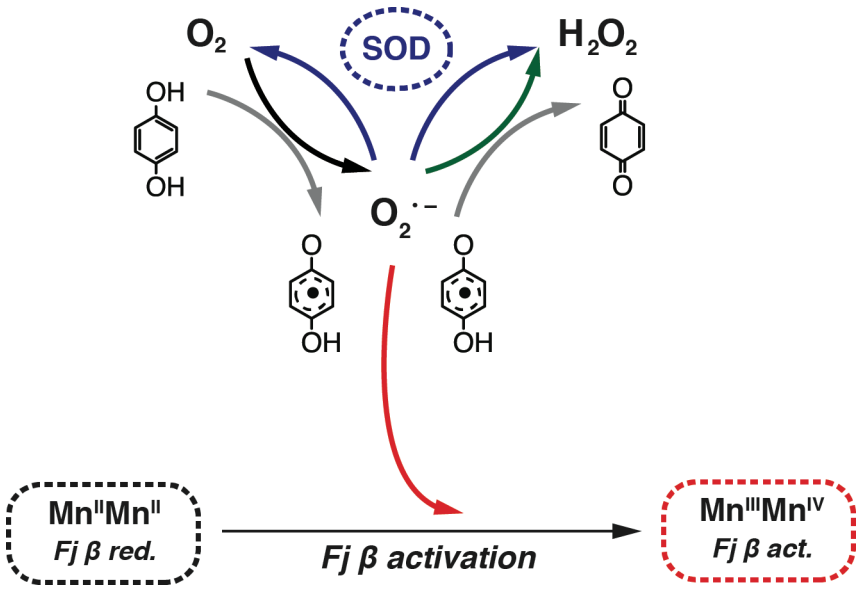

Scheme S1. Reactions involved in the activation of *Fj* RNR-β by superoxide generated from hydroquinone and O_2. Quinol (hydroquinol or naphthoquinol) reacts with oxygen to form semiquinone and superoxide. The superoxide can then partition among three possible pathways: ***red,*** superoxide oxidizes the *Fj* RNR-β $Mn_2^{II/II}$ cluster to activate the protein; ***green,*** superoxide accepts another electron from the semiquinone to produce hydrogen peroxide and fully oxidized quinone; ***blue***, superoxide undergoes disproportionation, spontaneously or catalyzed by SOD, to produce O_2 and hydrogen peroxide. While the semiquinone is also capable of reacting with another equivalent of O_2 to form a second equivalent of superoxide and oxidized quinone (not shown), the observation that one or more equivalent of NQ is required to oxidized all the $Mn_2^{II/II}$ cluster suggests that this route is not predominant.

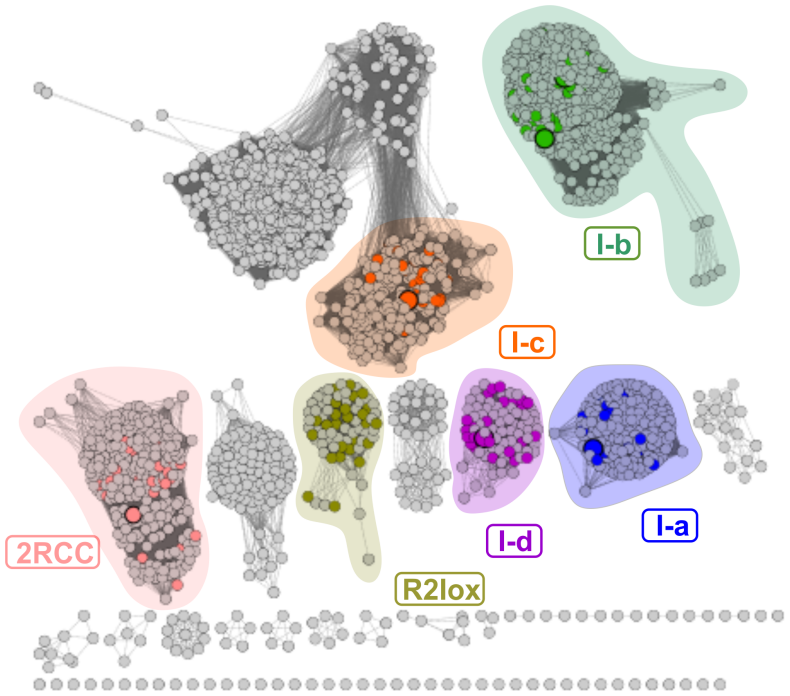

Figure S1. Sequence similarity network (SSN) for the IPR000358 superfamily that contains the class I RNR β subunits. It was constructed with a minimum alignment score of 90. Each node represents a set of sequences with ≥ 90% identity. The nodes have been arranged in the organic layout. The colored nodes correspond to all sequences that were employed in the phylogenetic analysis. The larger nodes represent βs that include biochemically and/or structurally characterized representatives: *Escherichia coli* (Ia), *Bacillus subtilis* and *Corynebacterium ammoniagenes* (Ib), *Chlamydia trachomatis* (Ic), *Flavobacterium johnsoniae* (Id), *Bacillus halodurans* (PDB accession code 2RCC).

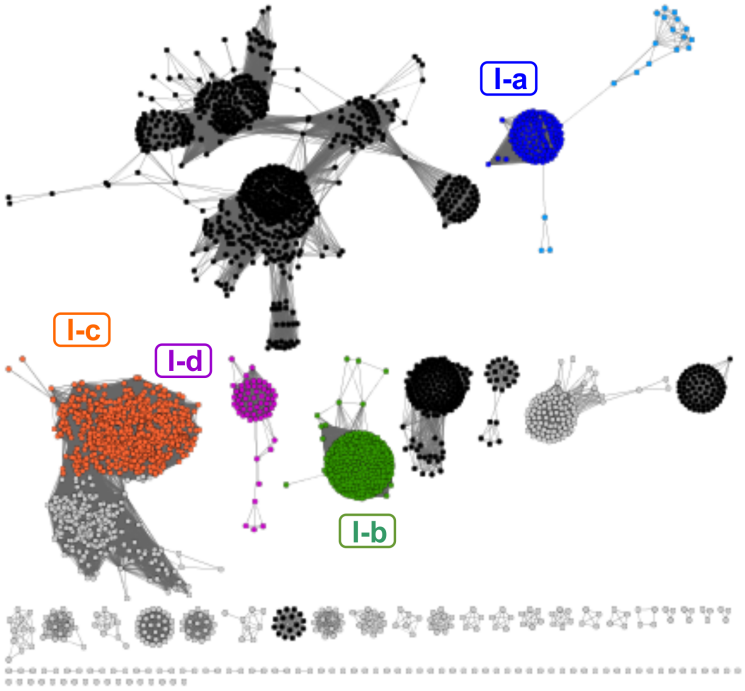

Figure S2. SSN for the ribonucleotide reductase α subunit superfamily generated with a minimum alignment score of 140. Each node represents a set of sequences with ≥ 85% identity. The nodes have been arranged in the organic layout. The highlighted nodes represent the sequences that were utilized in the phylogenetic analysis of the class I RNRs shown in Figures 5B, S22, and S23. The black nodes represent class II RNRs.

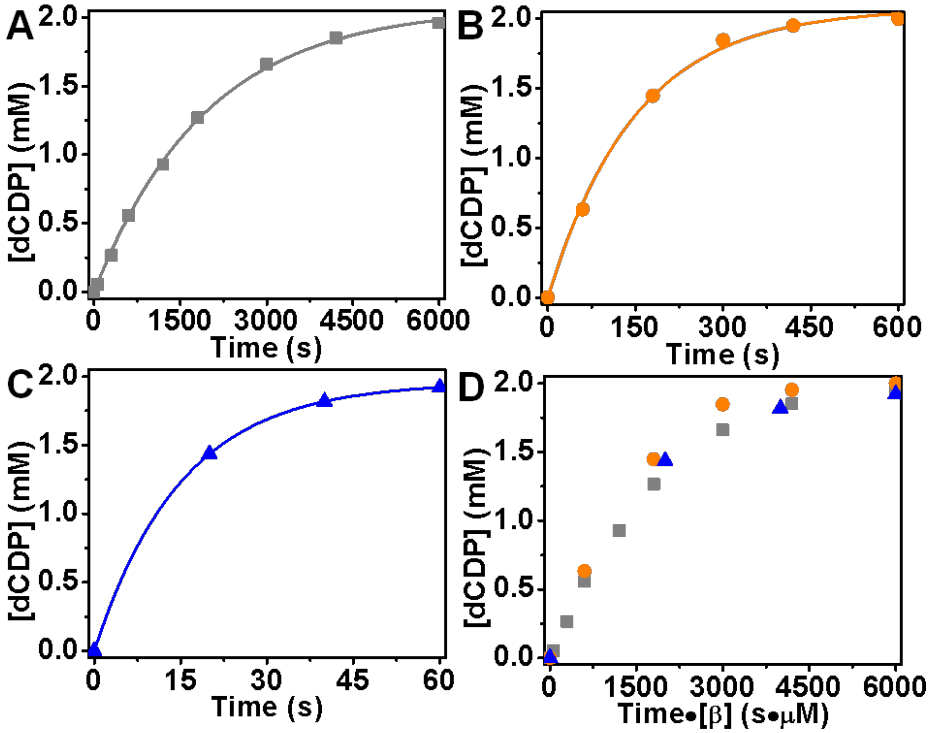

Figure S3. Comparison of the catalytic activities of *Fj* RNR at different concentrations of β and ten-fold excess of α. Plots of [dCDP] versus time at **(A)** 1 μM β, **(B)** 10 μM β, and **(C)** 100 μM β. **(D)** Plot of [dCDP] versus (time • [β]) to verify expected proportionality to enzyme concentration. In all activity assays, metal-depleted β was treated aerobically with 1.5 Mn^{II}/β followed by 1 NQ/β to activate the subunit.

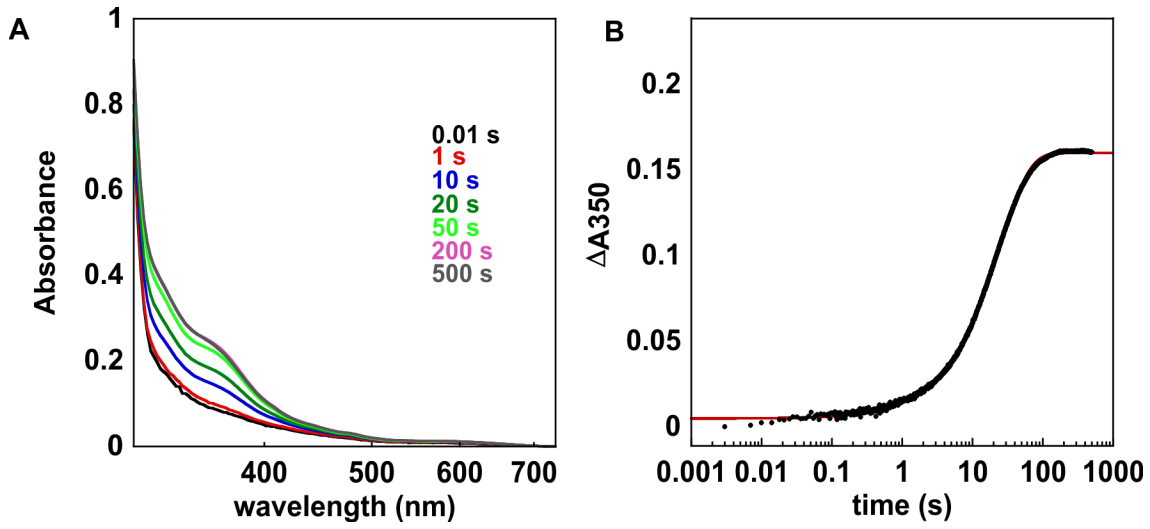

Figure S4. Reaction of the presumptive $Fe_2^{II/II}$ form of *Fj* β with O_2 monitored by stopped-flow absorption spectroscopy. A solution containing 0.40 mM *Fj* β was mixed at 5 °C with an O_2-saturated solution of 100 mM sodium HEPES (pH 7.5) buffer (1.8 mM O_2). The iron-loaded form of *Fj* β was isolated from *Ec* cells grown in M9 medium supplemented with Fe. After purification, the protein contained 0.6 Fe/β. The cofactor was reduced to the $Fe_2^{II/II}$ state by treatment in the absence of O_2 with a 10-fold excess of sodium dithionite, which was removed prior to the stopped-flow experiment by chromatography on a PD-10 column (GE Healthcare Bio-Sciences, Pittsburgh, PA). **(A)** Selected absorption spectra acquired at reaction times indicated in the figure. **(B)** ΔA_{350}-versus-time trace depicting the kinetics of oxidation of the cofactor to the $Fe_2^{III/III}$ form. The red line is the result of a regression fit of the equation for an exponential growth to the data. It corresponds to k_{obs} = 0.04 s^{-1}.

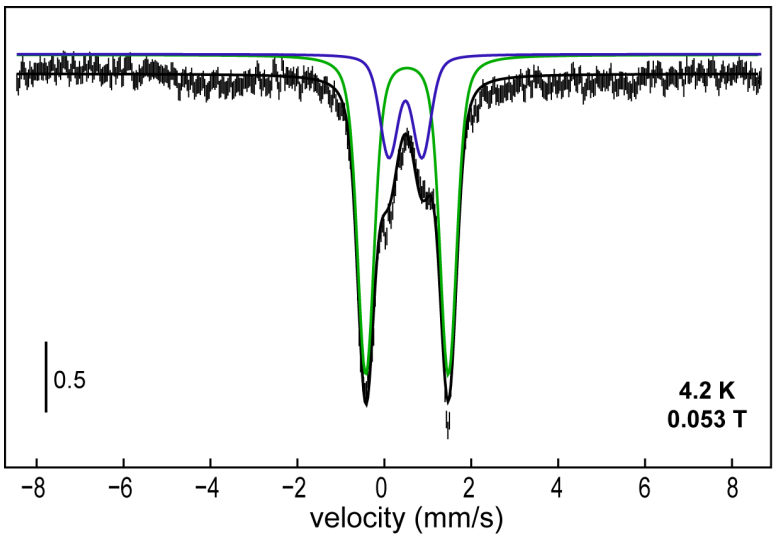

Figure S5. 4.2-K/53-mT Mössbauer spectrum of a sample of *Fj* β purified from *Ec* BL21(DE3) cells grown in M9 (minimal) medium supplemented with ^{57}Fe. The sample contained 0.6 Fe/β. Approximately 85% is in the form of antiferromagnetically coupled (S_{tot} = 0) $Fe_2^{III/III}$ clusters (green and purple theoretical traces), whereas the remainder is in the form of mononuclear high-spin Fe^{III} (S = 5/2). The theoretical traces correspond to quadrupole doublets with parameters δ_{av} = 0.52 mm/s, ΔE_{Qav} = 1.90 mm/s (~ 64% of the total intensity) and δ = 0.49 mm/s, ΔE_Q = 0.76 mm/s (~ 21% of the total intensity). The applied magnetic field was oriented parallel to the γ beam.

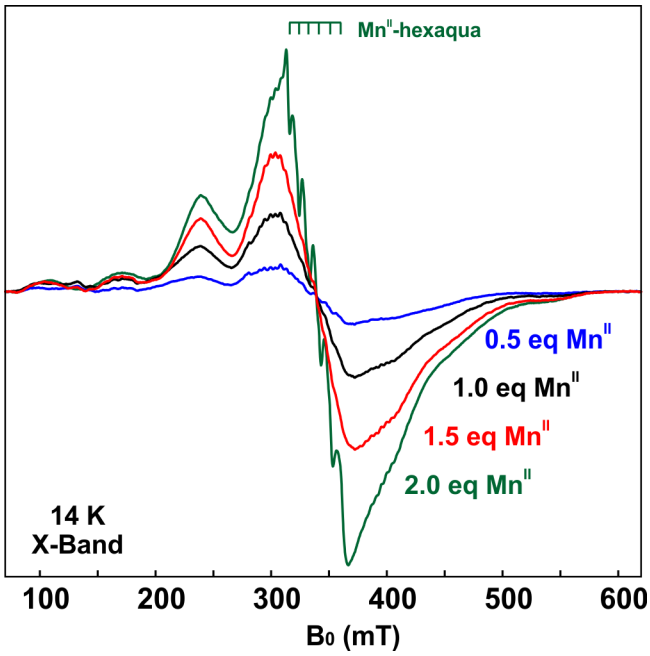

Figure S6. Titration of 0.30 mM metal-depleted *Fj* RNR β with Mn^{II} monitored by CW EPR spectroscopy. The equivalencies quoted are *total* Mn/β – the sum of that present after purification and that added in the titration. Metal analysis indicated that the protein had 0.17 Mn/β and 0.25 Fe/β at the start of the experiment. Spectrometer conditions: temperature = 14 K, microwave power = 2 mW, modulation amplitude = 1 mT, microwave frequency = 9.480 GHz, number of points = 2048.

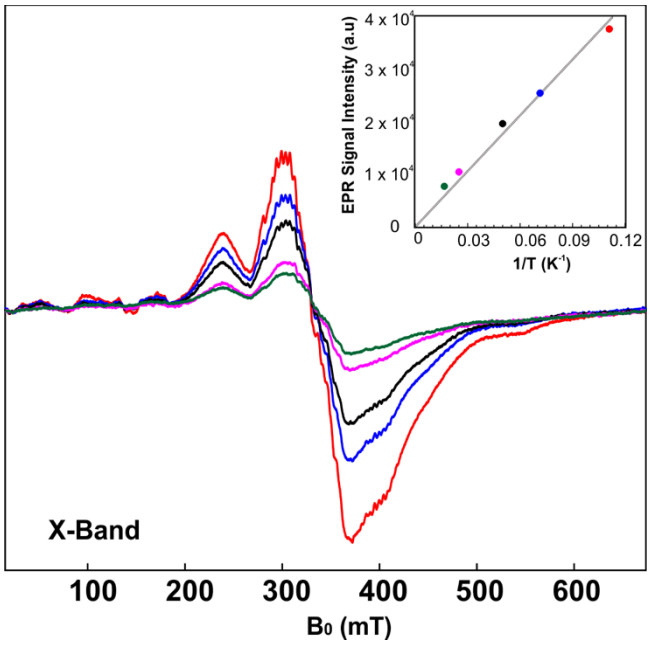

Figure S7. CW EPR spectra of a sample containing 0.30 mM *Fj* β and 2 Mn^{II}/β recorded at 8 K (red trace), 14 K (blue trace), 20 K (black trace), 42 K (magenta trace), and 60 K (green trace). *Inset*: EPR signal intensity as a function of the reciprocal of the temperature (1/T, K^{-1}). The data points are colored to match the corresponding EPR spectra. Experimental conditions: microwave power = 2 mW, modulation amplitude = 1 mT, microwave frequency = 9.480 GHz, number of points = 4096. The metal-depleted protein used in the experiment was isolated with 0.17 Mn/β.

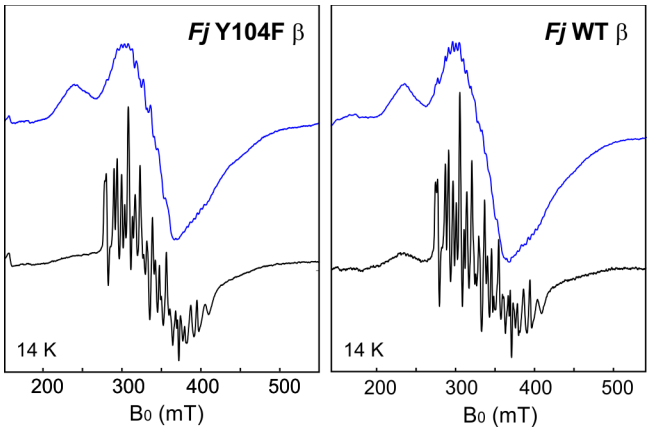

Figure S8. X-band CW EPR spectra of samples containing 0.40 mM of the Tyr^{104}Phe (left) or WT (right) *Fj* β protein and 1 Mn^{II}/β. *Blue trace*, before reaction with NQ; *black trace*, after reaction of the air-saturated samples with 1 NQ/β, as described. Experimental conditions: microwave power = 2 mW, microwave frequency = 9.480 GHz, modulation amplitude = 1 mT, temperature = 14 K, scan time = 169 s.

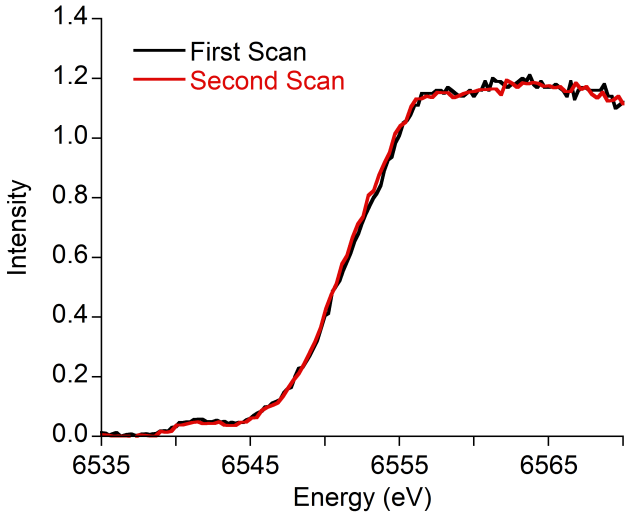

Figure S9. Overlay of the first and second XAS scans of activated *Fj* β, demonstrating that the sample is undamaged by the first scan.

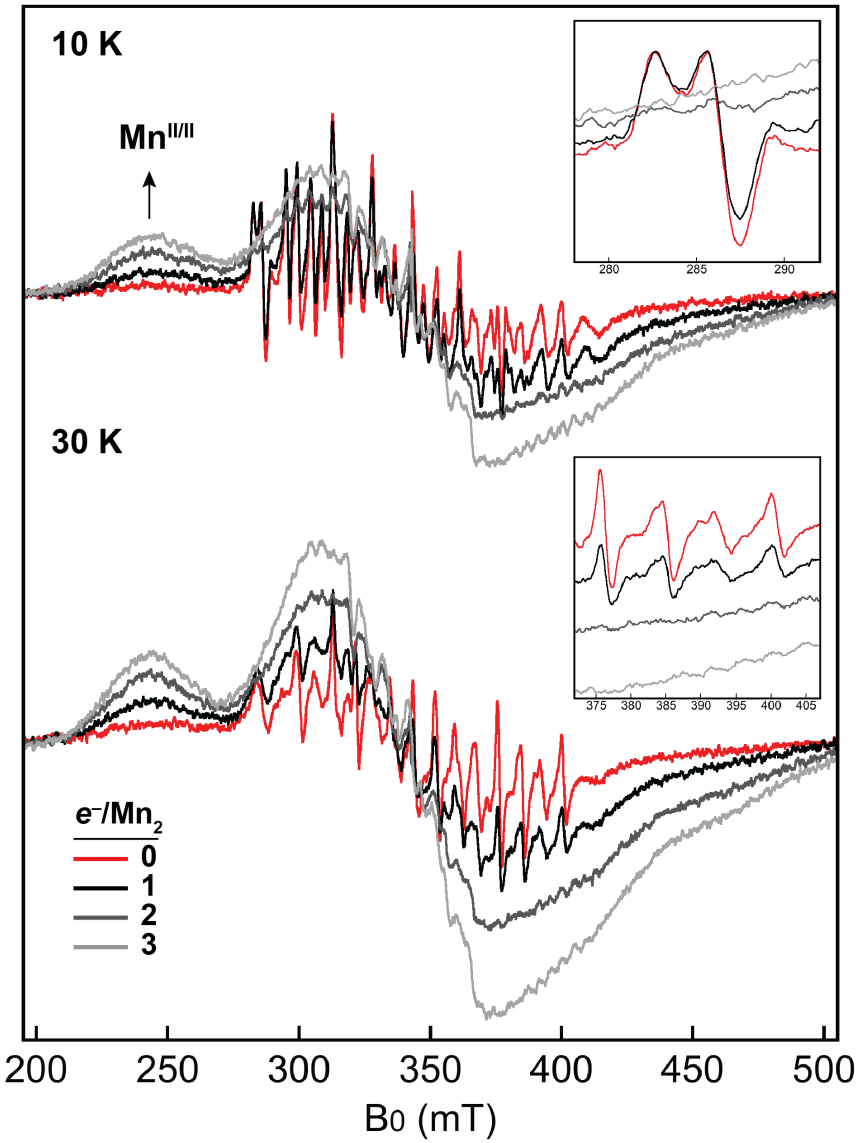

Figure S10. Anoxic titration of 0.34 mM activated *Fj* β with sodium dithionite monitored by CW EPR spectroscopy. Small aliquots of a freshly prepared, standardized ~ 4 mM solution of dithionite were added in the absence of O_2 to a larger volume of the protein. After addition of the reductant, samples were incubated for 5 min at 21 ± 2 °C prior to freezing. Reducing equivalents are relative to the concentration of the Mn_2 cofactor (0.21 mM, as determined by ICP-AES). ***Top inset,*** blow-up of region used to quantify complex ***1*** remaining in each sample. ***Bottom inset,*** blow-up of region used to quantify complex ***2*** remaining in each sample. Spectrometer conditions: microwave frequency = 9.625 GHz, modulation amplitude = 5 mT, microwave power = 2 mW, temperature = 10 K and 30 K, scan time = 320 s.

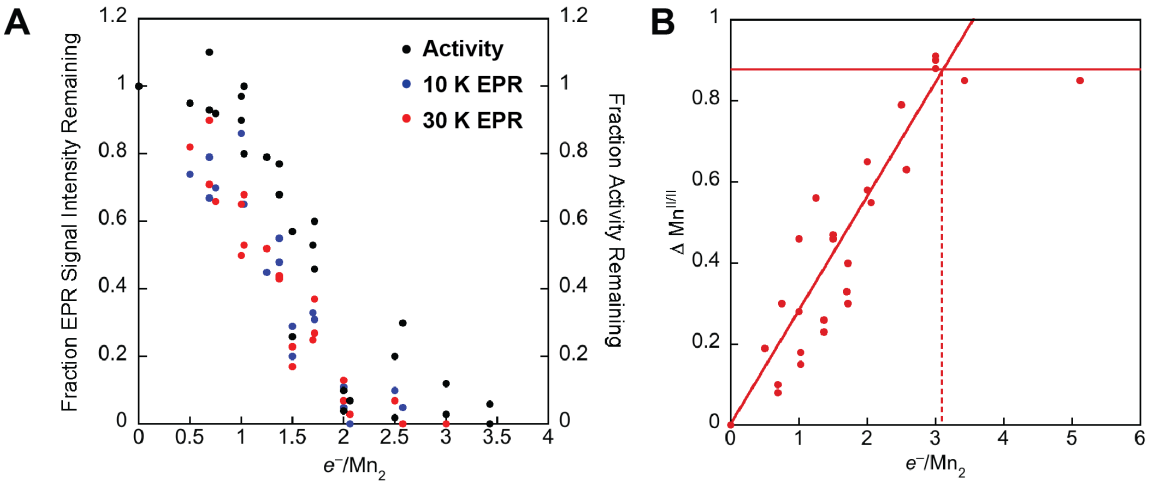

Figure S11. EPR evidence that reduction of the oxidized dimanganese clusters in activated *Fj* β is correlated with loss of catalytic activity and appearance of the $Mn_2^{II/II}$ complex. **(A)** Fraction of EPR signal intensity and activity remaining as a function of reducing equivalents added in all titrations of activated *Fj* β with sodium dithionite. Reducing equivalents are relative to the Mn_2 cofactor concentration in each sample, and EPR spectra were measured as in Fig. S10. Activity was measured at 40 μM β,in the absence O_2 and in the presence of 40 μ*M* Vu SOD. **(B)** Quantification of the $Mn_2^{II/II}$ complex from the broad feature from 200-270 mT. The intensity exhibited by the sample with the maximum quantity of dithionite was set to 100%.

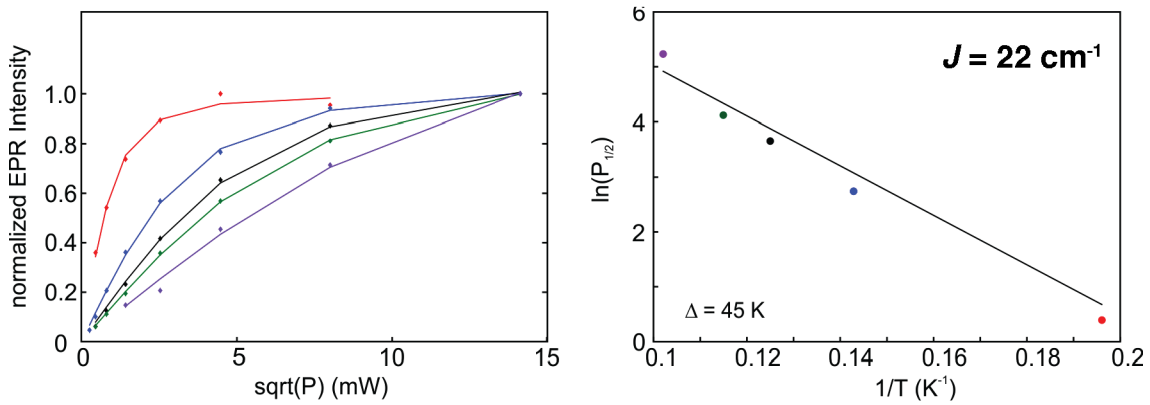

Figure S12. Use of the power and temperature dependence of the EPR signal associated with complex ***1*** to estimate its exchange coupling constant, *J*. (***Left***) plots of signal intensity versus power at temperatures 5.1 (*red*), 7 (*blue*), 8 (*black*), 8.7 (*green*) and 9.8 (*purple*) K. (***Right***) plot of the natural logarithm of $P_{1/2}$ (half the microwave power required for the onset of saturation of the signal) versus reciprocal temperature (1/T). Each data point was obtained by least-squares fitting of the experimental power saturation curves obtained from the data in the left panel. *J* is estimated to be ~ 22 cm^{-1} based on the assumption that the first excited spin state (S_{tot} = 3/2) is at an energy Δ ~ 3/2*J* ($H_{ex} = J\,\mathbf{S_1}\cdot\mathbf{S_2}$) above the S_{tot} = 1/2 ground state.

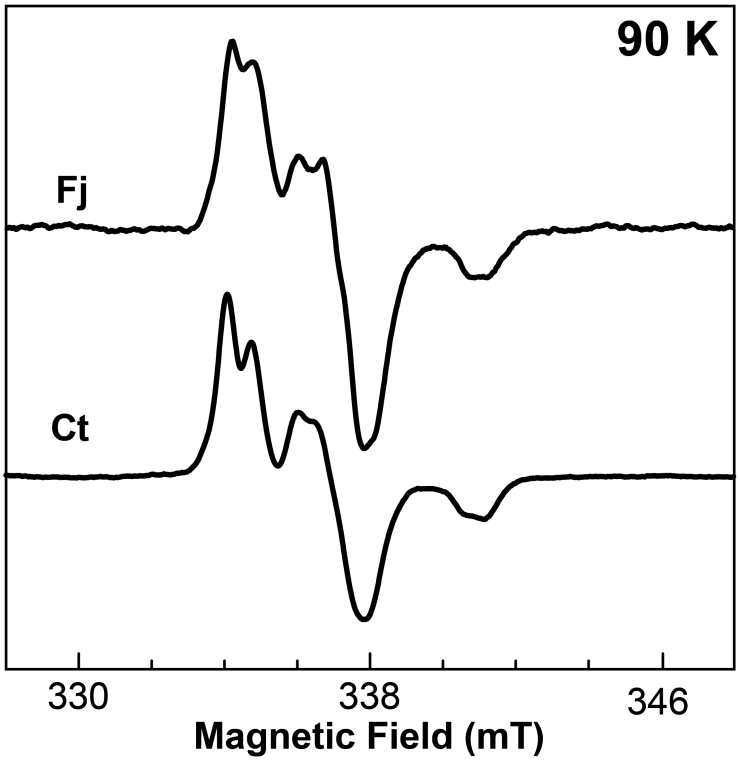

Figure S13. EPR spectra at 90 K showing the signature of the nitrogen-centered radical (N•) generated from 2'-azido-2'-deoxyribonucleotide (N_3-UDP) by *Fj* RNR and the class Ic *Ct* RNR.[11]

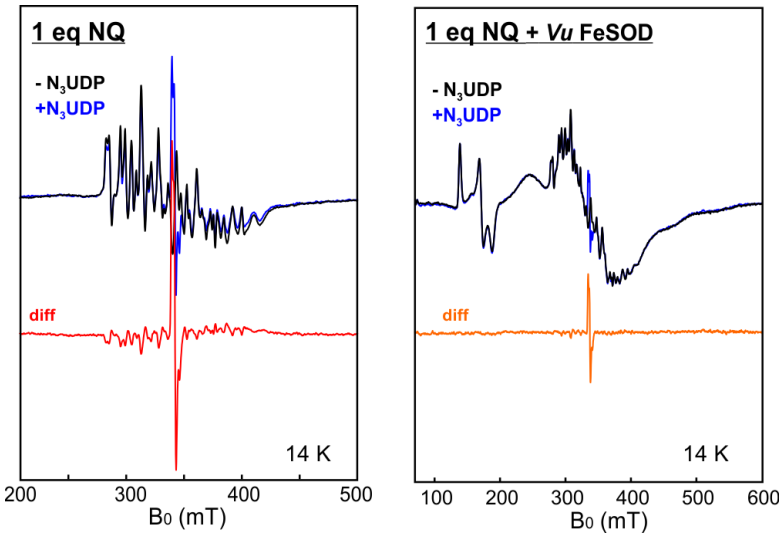

Figure S14. X-band EPR evidence that *Vu* SOD suppresses activation of β by NQ/O_2. SOD inclusion during protein activation also results in diminished formation of the nitrogen-centered radical (N•) upon subsequent treatment of the *Fj* RNR holoenzyme with the radical-trapping mechanism-based inactivator, N_3-UDP. (***Left***) treatment with N_3-UDP of the holenzyme formed from β that had been activated by the optimized procedure with NQ in the absence of *Vu* SOD. ***Black***, before treatment with N_3-UDP. ***Blue***, after treatment with 0.9 mM N_3-UDP for 90 s at 21 ± 2 °C in the presence of 3 α/β and 1 mM ATP. ***Red***, difference spectrum showing features that form (positive) and decay (negative) as a result of the reaction with N_3-UDP. (***Right***) treatment with N_3-UDP of the holoenzyme assembled with β activated by the same procedure but with inclusion of 0.14 mM *Vu* SOD, color-coded as in the left panel. Spectrometer conditions: microwave frequency = 9.48 GHz, modulation amplitude = 0.6 mT, microwave power = 2 mW, scan time = 169 s, temperature 14 K.

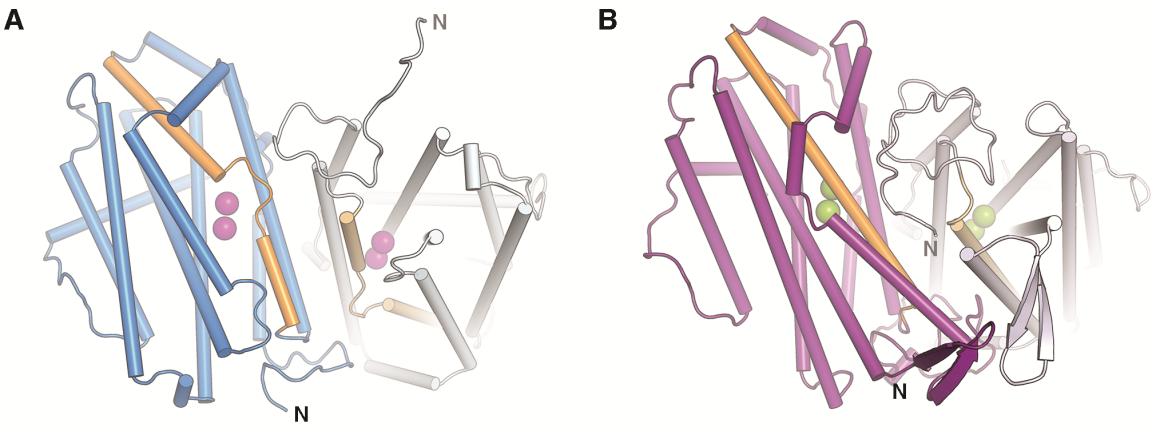

Figure S15. Conservation of quaternary structure among *Fj* β_2 and other structurally characterized class Ia-c β subunits. (**A**) Ribbon diagram of the structure of *Fj* β_2. (**B**) Corresponding diagram of the *Ec* class Ia $Fe_2^{II/II}$- β_2 (1PIY PDB accession code). Mn and Fe ions are illustrated as purple and green spheres, respectively. Core helix α1, containing Glu 67 and Lys 71 in *Fj* β, is highlighted in orange and the second β subunit is shown in gray.

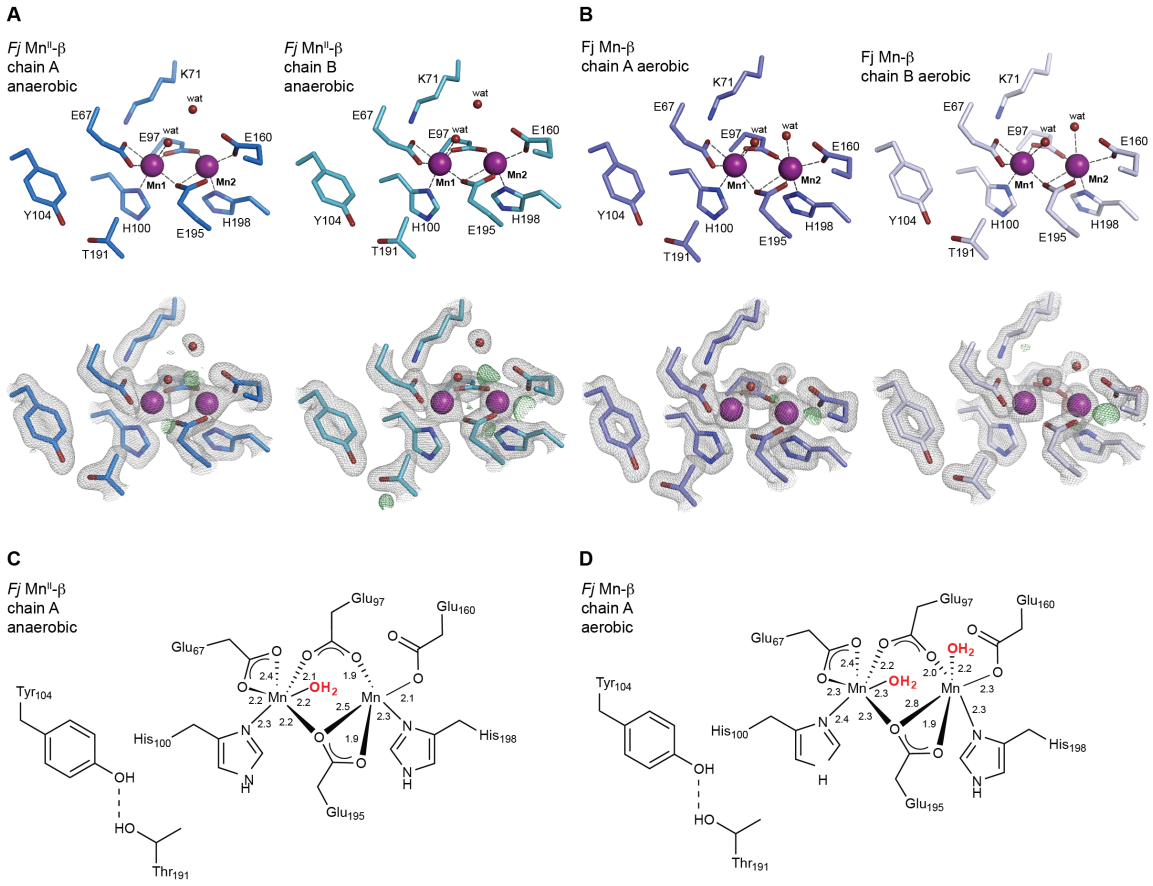

Figure S16. Views of the active site models and electron density maps ($2F_o$-F_c electron density map in gray mesh, contoured at 2.0 σ, and F_o-F_c electron density map in green mesh, contoured at 3.0 σ) in the two chains of *Fj* β_2 from structures obtained by two different procedures. (**A**) Structure obtained by anoxic Mn^{II} soaking of crystals of *Fj* β_2. (**B**) Structure obtained by co-crystallization with Mn^{II} in air. Selected amino acid side chains are shown in ball and stick format, water molecules are shown as red spheres, and Mn ions are shown as purple spheres. Little difference density is observed when metal-stripped protein is co-crystallized or soaked with Mn^{II}, indicative of a well-ordered and fully-occupied metal binding site. (**C** and **D**) Schematic diagrams with distances shown in Å.

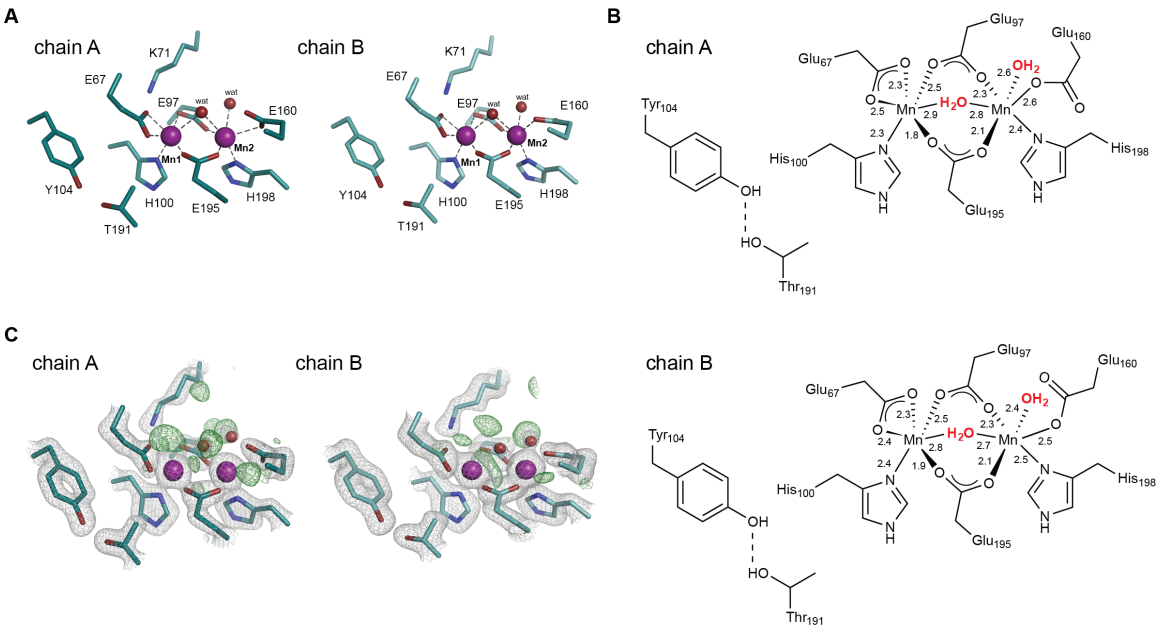

Figure S17. *Fj* β_2 active site model obtained from crystals of the as-isolated Strep-tagged protein. (**A**) Structural model of each chain. Selected amino acid side chains are shown in ball and stick format, water molecules are shown as red spheres, and Mn ions are shown as purple spheres. (**B**) Schematic of the metal-ligand interactions in each chain, with distances shown in Å. (**C**) $2F_o$-F_c electron density map (gray mesh, contoured at 2.0 σ) and F_o-F_c electron density map (green mesh, contoured at 3.0 σ) for active site residues in each chain. The difference density is likely a consequence of photoreduction or inherent heterogeneity in the structure of assembled metal cluster when generated inside the cell or during protein isolation. This second 1.9-Å-resolution structure of *Fj* β was obtained by aerobic crystallization of protein isolated from cultures grown in minimal medium supplemented with Mn^{II}, a procedure that affords enzymatically active protein ($v/\beta \sim 0.74\ s^{-1}$) and yields a nearly fully occupied (> 85%) Mn_2 binding site in the x-ray crystal structure. We anticipated that comparison of this structure to the anaerobic Mn^{II}-soaked metal binding site (Fig. S16) might provide insight into the structure of the Mn_2 cluster after activation. Among the ligands provided by the protein, the differences are confined to minor adjustments in the bridging Glu ligands. However, there are potentially more significant changes in the locations and coordination modes of non-protein ligands. Electron density maps obtained from crystals prepared from metal-depleted protein to which Mn^{II} was added anaerobically invariably have an intense lobe

near metal site 1 that is reasonably modeled in this structure as a Mn1-coordinated water molecule. The presence of this ligand renders Mn1 six-coordinate, while the five-coordinate Mn2 retains one open position *trans* to His 198. Interestingly, the distinctions between as-isolated and anaerobically-reconstituted Mn^{II}-bound *Fj* β are also reflected in a third structure in which metal-stripped protein was crystallized with Mn^{II} under aerobic conditions (Fig. S16), suggesting that activated *Fj* β may accumulate via slow scavenge of superoxide during aerobic crystallization. The datasets obtained from crystals simultaneously exposed to Mn^{II} and O_2 now have two lobes of density present in slightly different locations, also modeled as waters. One lobe is between the Mn ions and appears to arise from an oxygen bridge (OH_x; x = 0-2), while the other is solely associated with Mn2 and likely arises from a terminal OH_x ligand. In the structure of the as-isolated protein, the Mn2 ligand can be definitively modeled *trans* to Glu 195, an arrangement not previously observed in any other RNR β structure. In this position, the new ligand projects into the solvent channel (Figs. 4D, S19), toward the site of a Mg^{II} ion at the dimer interface. These additional structures fail to provide support for acquisition and/or transformation of an exogenous redox-active ligand in the cavity during activation. However, they do suggest that superoxide may add initially to the open sites on Mn2, as delineated by the positions of the exogenous ligands in the structures from O_2-exposed crystals, a phenomenon potentially driven by initial protection of the open coordination site on Mn1 in the $Mn_2^{II/II}$ state.

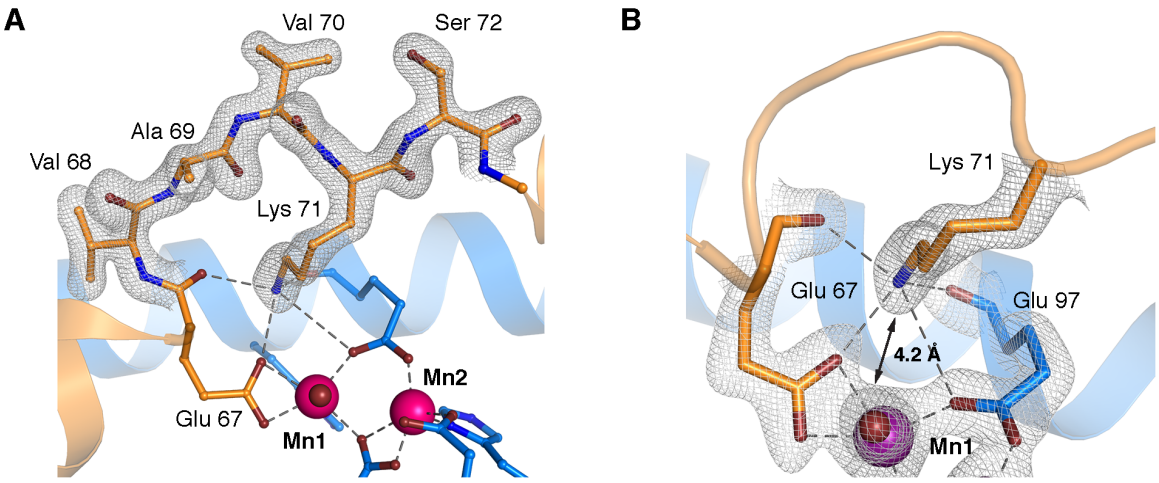

Figure S18. (**A**) The backbone in a segment of core helix 1 immediately following Glu^{67} (residues 68-72) converts from an α-helical hydrogen-bonding arrangement to a β-strand pattern. (**B**) A zoomed-in view of the backbone and side chain hydrogen-bond acceptors for the Lys 71 ε-NH_3^+ functional group. The Lys 71 residue is constrained to a position 4.2 Å away from Mn1. Selected amino acids are shown in ball and stick format, water molecules are shown as red spheres, and Mn ions are represented as purple/pink spheres. A $2F_o$-F_c electron density map is shown in gray mesh, contoured at 1.5 σ.

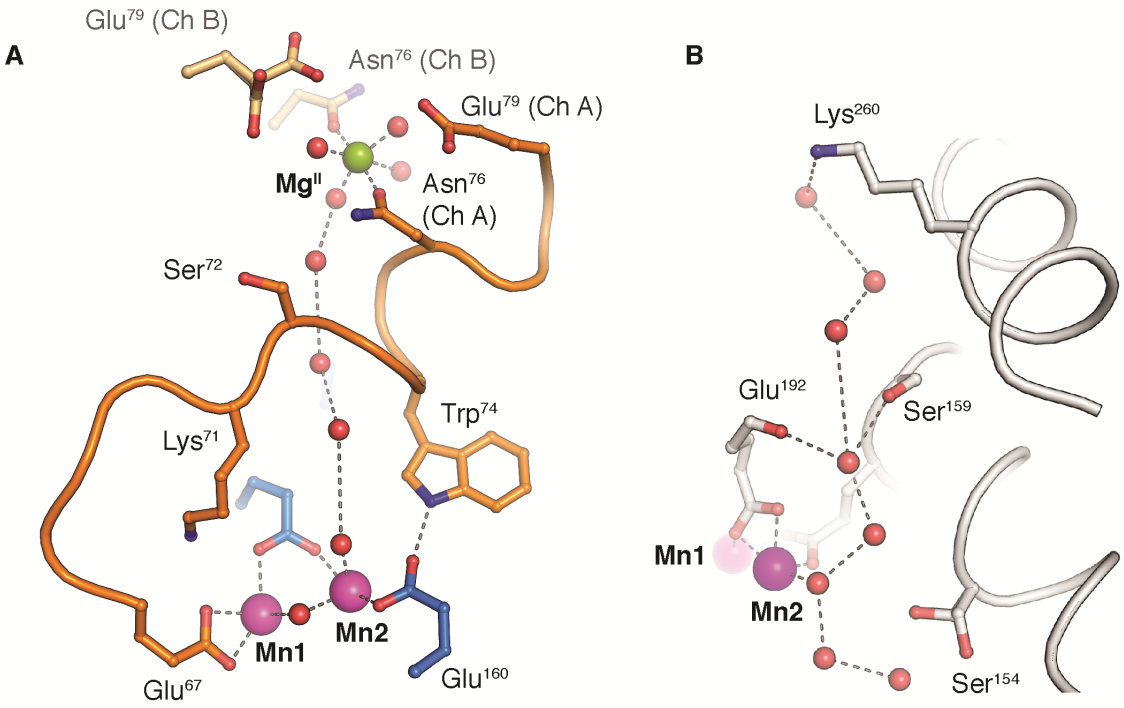

Figure S19. (**A**) Comparison of the water channel in *Fj* β to (**B**) a similar channel in *Ec* class Ib β (NrdF, PDB accession code 3N37). Selected amino acid side chains are shown in ball and stick format, water molecules shown as red spheres, and Mn ions are shown as purple spheres. The Mg^{II} ion in the *Fj* β structure is shown as a green sphere.

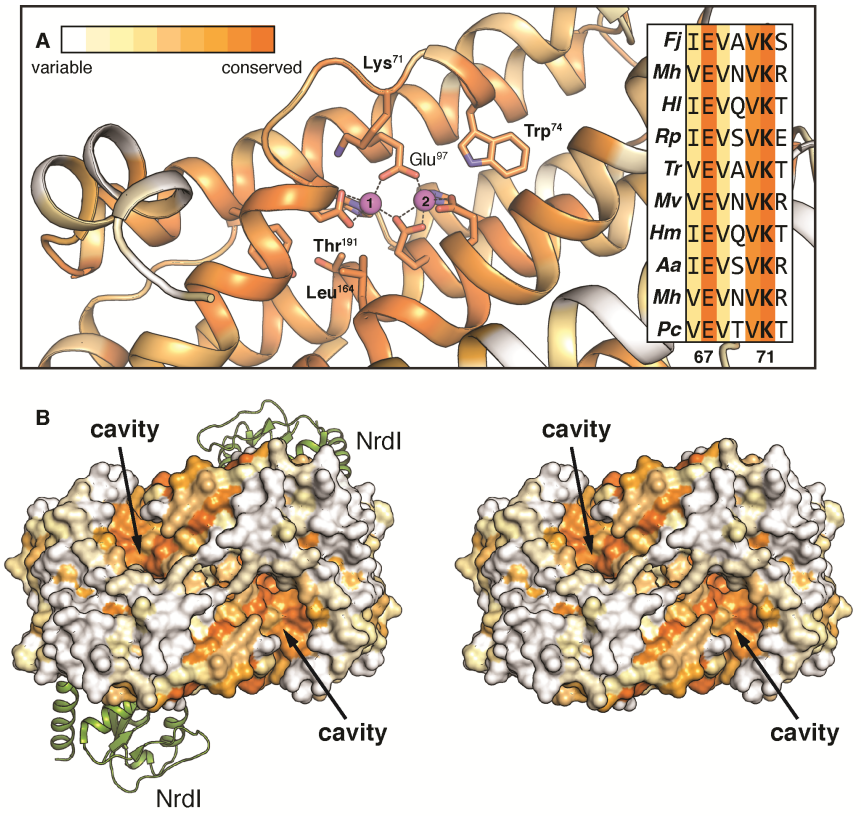

Figure S20. (**A**) Cutaway view of a Consurf map[12] of the cavity containing Lys 71 in *Fj* β, generated using a MUSCLE alignment of 259 class Id RNR β subunit sequences. Alignment of selected residues from a representative set of Id β sequences is shown in inset (*Fj* = *Flavobacterium johnsoniae*, *Mh* = *Mannheimia haemolytica*, *Hl* = *Halorubrum lacuprofundi*, *Rp* = *Rhizobium* phage, *Tr* = *Truepera radiovictrix*, *Mv* = *Mannheimia varigena*, *Hm* = *Halomicrobium mukohataei*, *Aa* = *Aggregatibacter actinomycetemcomitans*, *Mh* = *Mannheimia haemolytica*, *Pc* = *Porphyromonas catoniae*). The protein backbone is illustrated as a ribbon diagram, selected amino acid side chains are shown in ball and stick format, and Mn ions are shown as purple spheres. (**B**) Surface map of sequence conservation[12] in the vicinity of the cavity in the β_2 homodimer. Comparison of the cavity location against a docked model of *Fj* β with NrdI (green cartoon, *left*, generated using the *Ec* NrdI model from the NrdI•NrdF complex in PDB accession code 3N3A) shows that the NrdI binding interface does not overlap with the cavity and solvent channel (see Fig. S24 for additional comparison), perhaps consistent with a distinct route for superoxide access in *Fj* β.

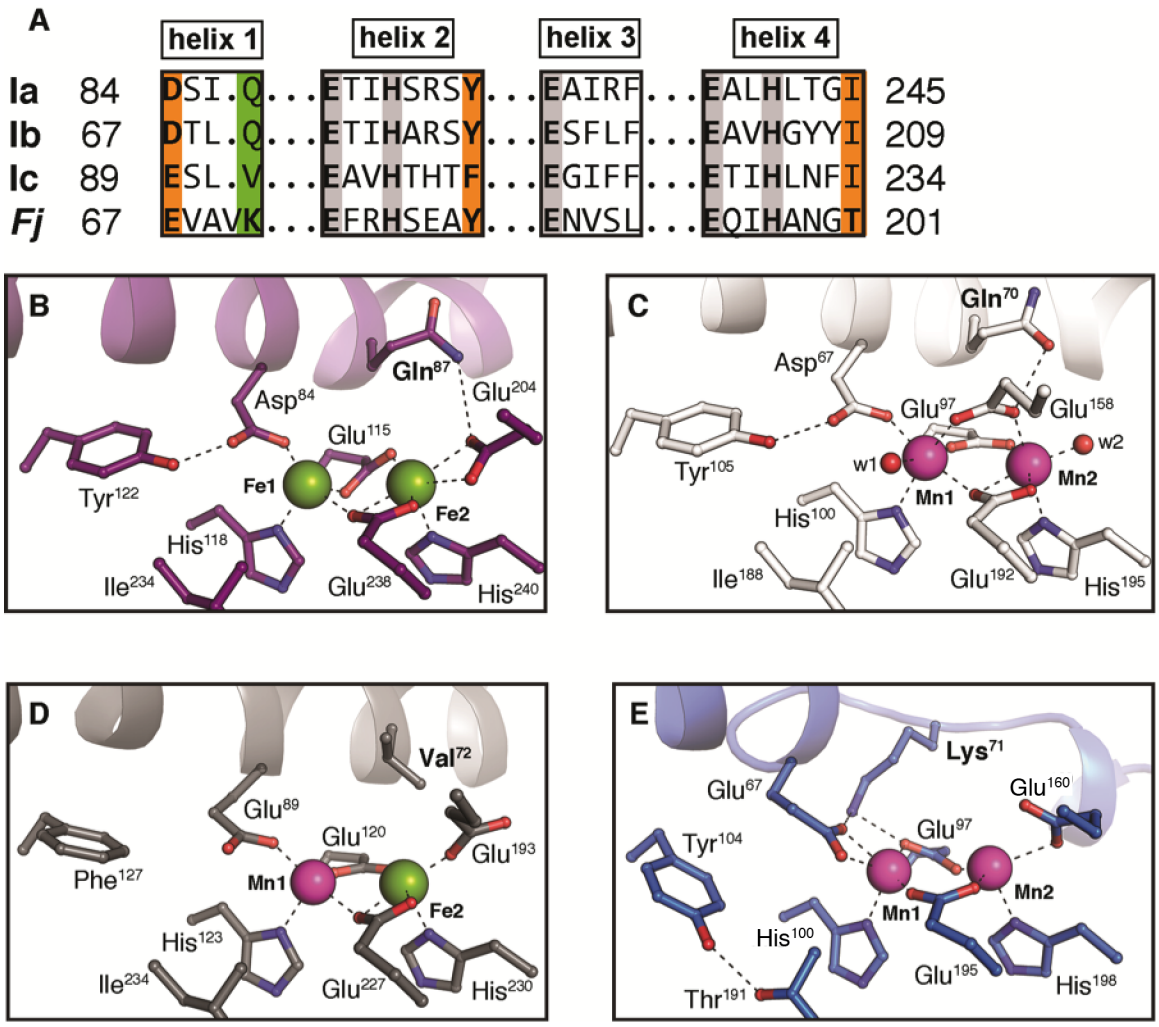

Figure S21. (***A***) Alignment of selected residues in *Fj* β with those in representative class Ia-c βs (Ia = *Ec*, Ib = *Ec*, Ic = *Ct*). Structural comparison of active-site regions, focusing on counterparts to Lys 71 (residue label in boldface), (***B***) in *Ec* class Ia β (1PIY PDB accession code), (***C***) *Ec* class Ib β (3N37 PDB accession code) (***D***), *Ct* class Ic β (4M1I PDB accession code), and (***E***) *Fj* β. Selected amino acid side chains are shown in ball and stick format, water molecules are shown as red spheres, and Mn/Fe ions are shown as purple/green spheres.

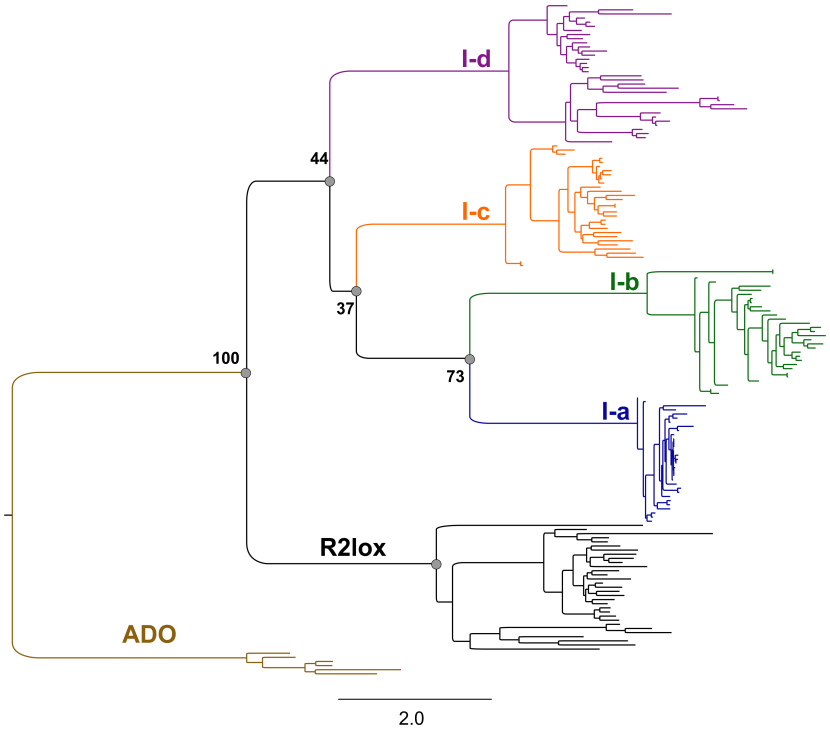

Figure S22. Maximum-likelihood (ML) rectangular rooted phylogenetic tree generated with the 157 sequences used for the construction of Fig. 5B but also including 6 sequences of aldehyde deformylating oxygenases (ADOs) as an outgroup. This analysis was carried out to evaluate the merit of the selection of the R2lox outgroup in generation of the phylogenetic scheme favored in the main text. The tree was computed with RaxML (version 7) using the LG model for the rate of heterogeneity, invariant sites, and empirical base frequencies. The bootstrap values, showing the confidence level for the nodes, have been included for the major branches. The scale bar represents the number of substitutions per site. Sequences were aligned using MUSCLE. The analysis supports the supposition that the R2Iox proteins emerged in a branch of the common lineage that diverged before the segregation of any of the class I RNR subclasses. The limited resolution of the current tree, which arises from the relatively small number of sequences analyzed and is reflected by the low bootstrap values, precludes firm conclusions about the evolutionary lineage. Specifically, we cannot determine solely from this analysis whether the c and d subclasses split off together from the a/b lineage or, instead, the d subclass separated from the others first. Structural comparisons favor the latter option, an initial divergence of the Id lineage.

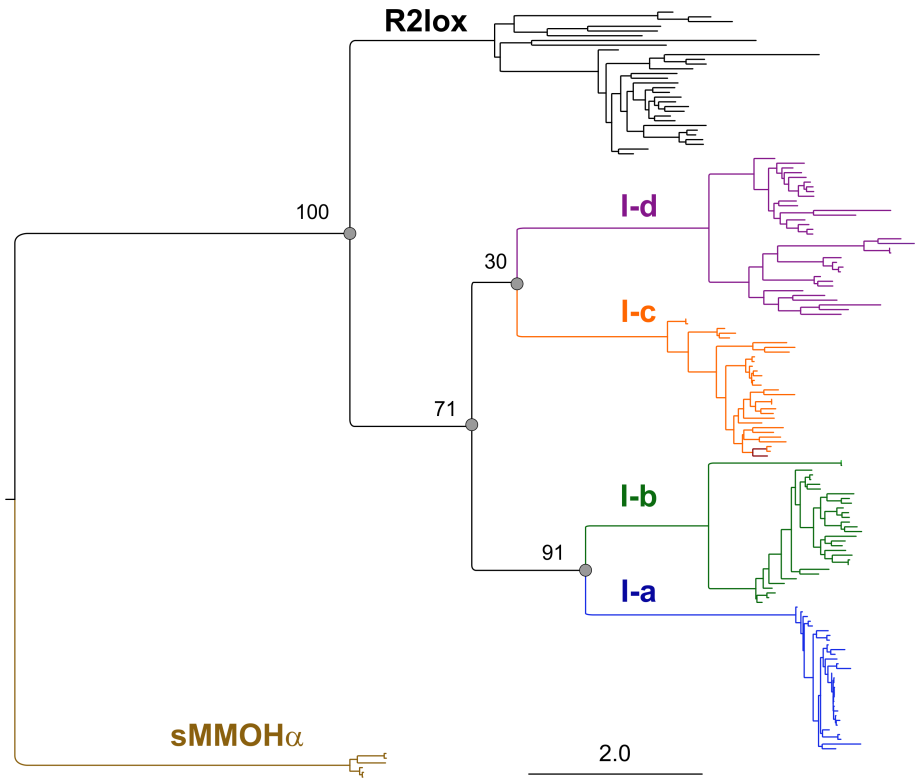

Figure S23. Maximum-likelihood (ML) rectangular rooted phylogenetic tree generated with the 157 sequences used for the construction of Fig. 5B but also including sequences of 6 soluble methane monooxygenase hydroxylase α subunits (sMMOHα) as an outgroup. This analysis was carried out to evaluate the merit of the selection of the R2lox outgroup in deduction of the phylogenetic scheme favored in the main text. The tree was constructed as described for Fig. S22.

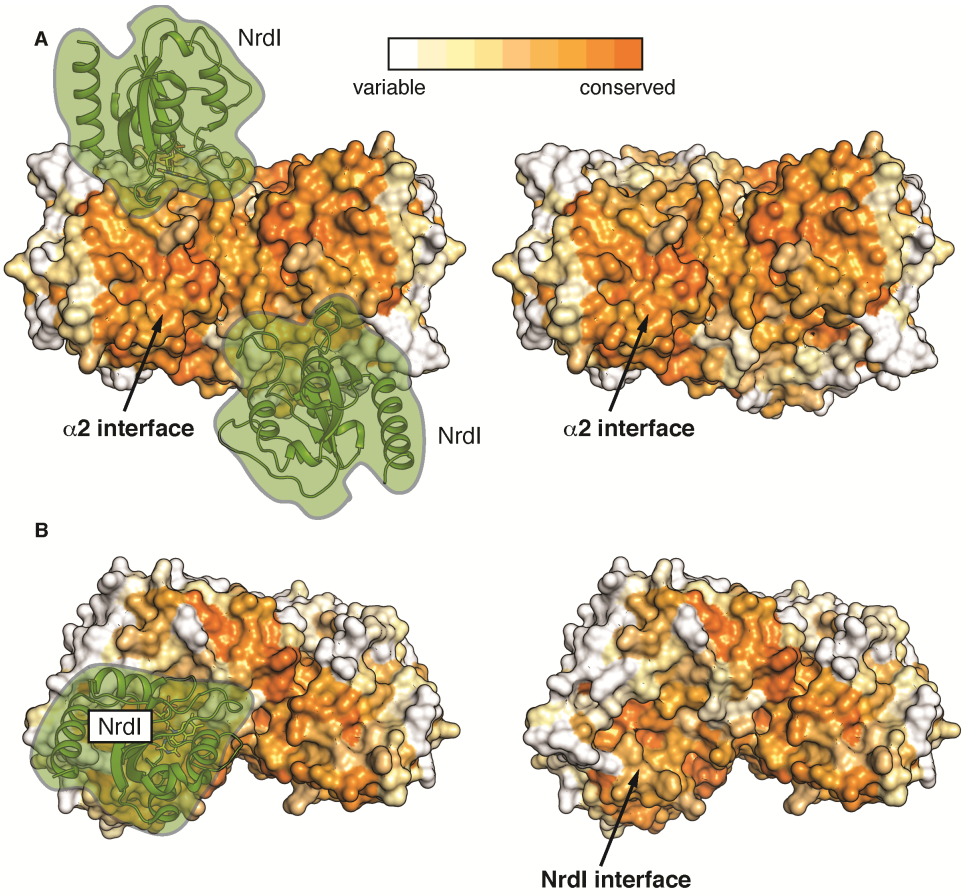

Figure S24. (**A**) Surface map of sequence conservation [12] for the predicted α_2 interface on *Fj* β_2, shown in comparison to the NrdI interface on *Ec* class Ib β_2 (green cartoon, ***left***, generated using the *Ec* NrdI model from the NrdI•NrdF complex in PDB accession code 3N3A, as in Fig. S20). (**B**) Analysis of the sequence conservation in the region of *Fj* β, analogous to the NrdI binding site in *Ec* class Ib β, and comparison to the cavity region (Fig. S20, panel **B**) or α_2 interface (**A**) shows a lesser degree of conservation, consistent with direct capture of superoxide instead of provision by NrdI at the equivalent interface.

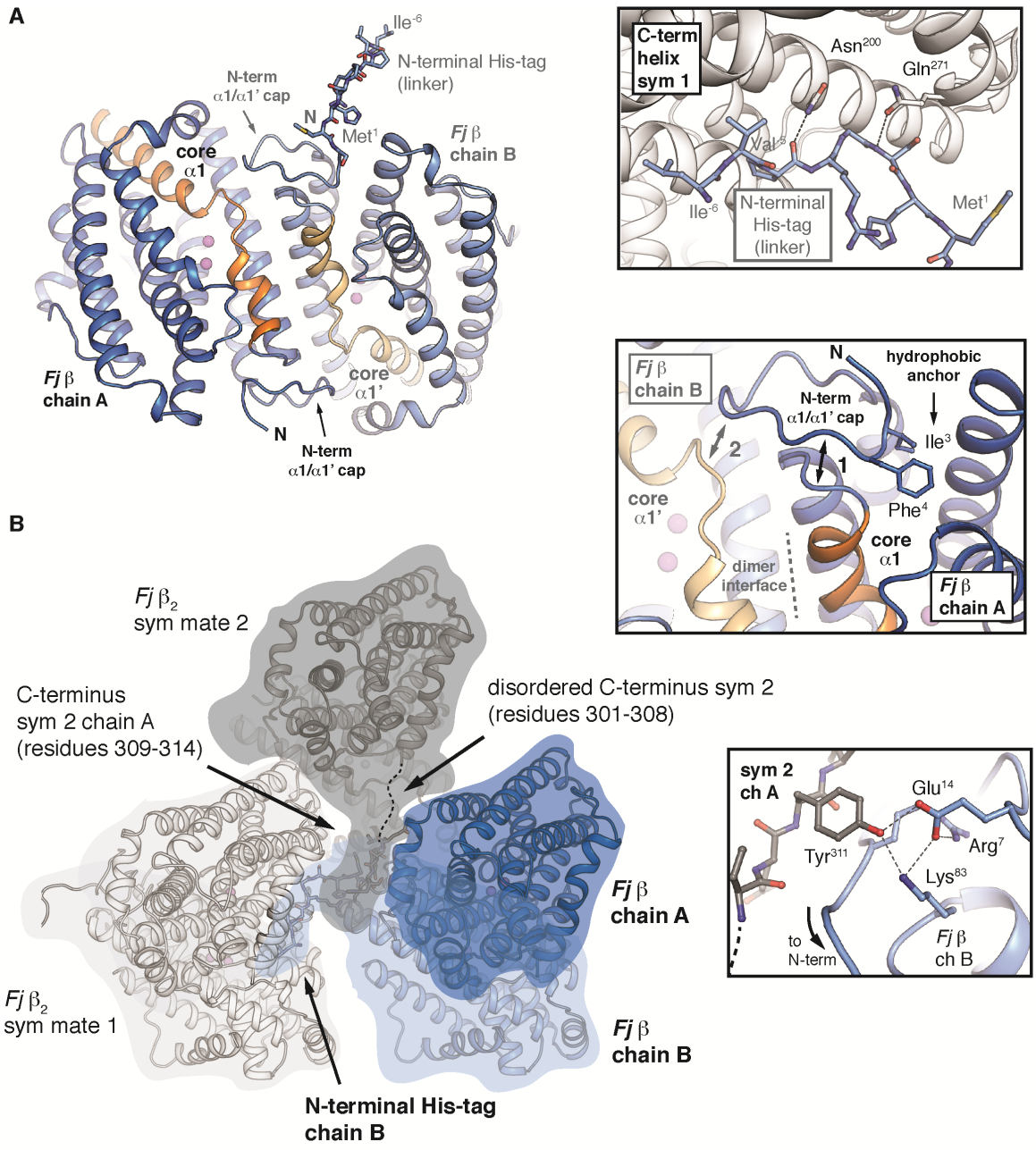

Figure S25. (**A**) The termini of *Fj* β stabilize the unfolded core helix and (**B**) are involved in crystal lattice interactions. (***Top right inset***) A crystal contact between the linker region of the N-terminal His_6 affinity tag in chain B (light blue ball-and-stick model) with the exterior of a neighboring symmetry mate (white ribbon diagram). (***Middle right inset***) The interaction does not alter the position of the N-terminus, firmly anchored in all structures (see Fig. S26) by a hydrophobic Ile 3-Phe 4 sequence. The

anchoring motif allows the residues that immediately follow this sequence to pack over the unfolded core α1 helix in the both monomers. A single terminus interacts with the C-terminal end of core helix α1 in the same monomer, in a capping interaction that may help stabilize the interrupted helix, as well as with the unfolded β-strand region in the adjacent monomer. The C-terminus of chain A facilitates crystal lattice contacts between a different pair of symmetry-related monomers. (***Lower right inset***) Residues 309-314 can be modeled in an interaction with a Lys-Glu pair near the N-terminus of chain B. Selected amino acid side chains are shown in ball-and-stick format and Mn ions are shown as purple spheres. Disordered regions are represented by dashed black lines.

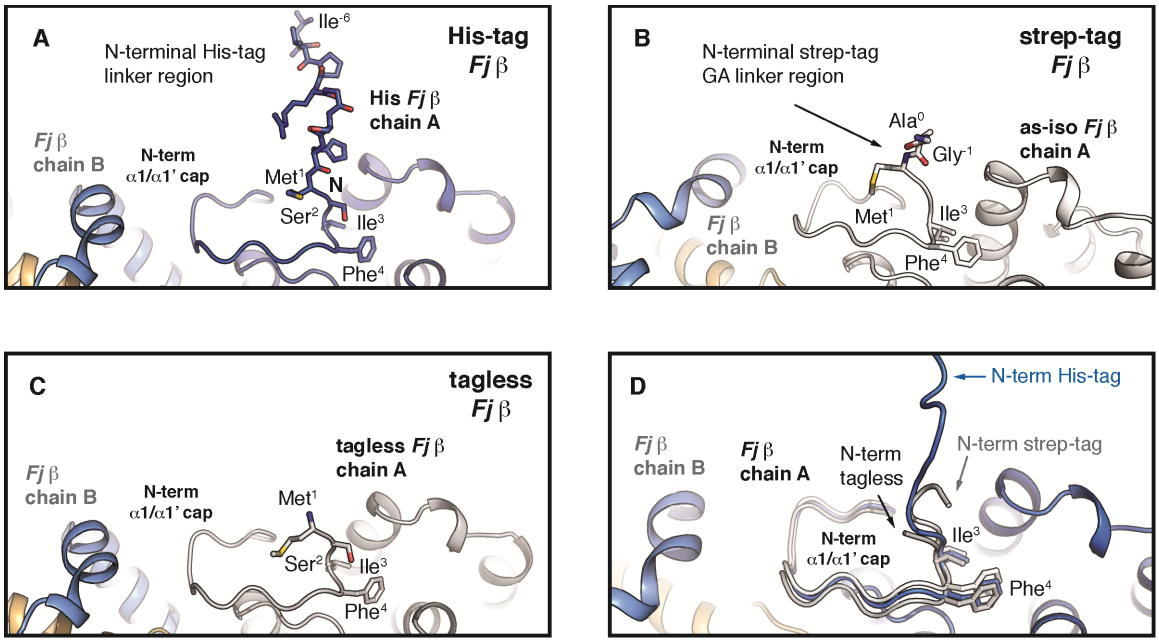

Figure S26. Comparison of the N-terminal regions in the crystal structures of affinity tagged *Fj* β proteins. (**A**) Structure of the hexahistidine-tagged *Fj* β. (**B**) Structure of the strep-tagged protein. (**C**) Structure of a tagless protein (not discussed here). (**D**) Overlay illustrating that the affinity tags have no impact on the position and structure of the N-terminal residues that follow Ile 3.

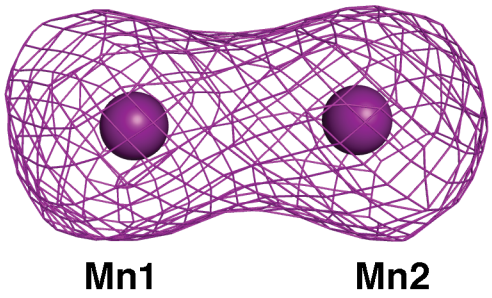

Figure S27. Anomalous difference Fourier map (purple mesh, contoured at 3.0σ) collected at the Mn absorption edge (Table S6) for as-isolated *Fj*-β.

Supplementary Tables

Table S1. Experimentally-determined metal stoichiometries for *Fj* β isolated by the different expression and purification procedures.

Procedure	Mn/β	Fe/β
1	0.17-0.25	0.07-0.25
2[a]	0.03-0.07	0.05-0.11
3	1.2-1.6	0.07-0.14
4	0.01-0.02	0.33-0.54

[a]Determined after reductive ferrozine chelation and EDTA treatment.

Table S2. Electronic and hyperfine parameters of the oxidized Mn_2 species generated in *Fj* β by the reaction of the protein with quinol and molecular oxygen.

		Mn^{III}			Mn^{IV}		
Species	**g-factors**	**A_1, MHz**	**A_2, MHz**	**A_3, MHz**	**A_1, MHz**	**A_2, MHz**	**A_3, MHz**
Complex *1*	1.96 1.94 2.008	-465	-435	-310	230	230	240
		Mn^{III}			Mn^{IV}		
Complex *2* [13]	2.002 1.97 2.01	-420	-420	-305	225	225	249

Table S3. Electronic and hyperfine parameters of characterized $Mn_2^{III/IV}$ complexes.							
		Mn^{III}			Mn^{IV}		
Source	**g-factors**	**A_1, MHz**	**A_2, MHz**	**A_3, MHz**	**A_1, MHz**	**A_2, MHz**	**A_3, MHz**
Ec class Ib RNR β (NrdF)[13]	2.008 2.008 1.980	-465	-435	-310	230	230	240
Tt Mn_2 catalase [14]	2.008 2.008 1.990	-420	-420	-305	225	225	249
Tt Mn_2 catalase [15]	2.014 2.014 2.00	-410	-425	-315	235	224	252
$[Mn^{III}Mn^{IV}(\mu\text{-}O)_2(PClNOL)_2]^+$ [16]	2.0014 2.003 1.986	-406	-466	-308	224	204	231
$[Mn_2(bipy)_4(\mu\text{-}O)_2](ClO_4) \bullet (H_2O)_2$ [16]	1.992 1.998 1.982	-483	-498	-378	214	211	231
$[Mn_2O_2(OAc)(HB(pz)_3)]$ [16]	2.001 2.002 1.985	-436	-474	-326	226	213	235

Table S4. Electronic and hyperfine parameters of characterized $Mn_2^{II/III}$ complexes.							
		Mn^{III}			Mn^{II}		
Source	**g-factors**	**A_1, MHz**	**A_2, MHz**	**A_3, MHz**	**A_1, MHz**	**A_2, MHz**	**A_3, MHz**
Tt Mn_2 catalase [16]	1.986 1.965 2.025	222	210	236	-529	-502	-730
$[Mn_2(bcmp)(p\text{-}OAc)_2](ClO_4)_2CH_2Cl_2$ [16]	1.905 1.905 2.022	219	219	318	-459	-459	-735
$[Mn_2(bpmp)(p\text{-}OAc)_2](ClO_4)_2 \bullet H_2O$ [16]	1.813 1.883 2.026	195	195	339	-435	-435	-801
$[Mn^{II}Mn^{III}(\mu\text{-}OH)\text{-}(\mu\text{-}piv)_2(Me_3tacn)_2]^{2+}$ [17]	1.964 1.947 2.022	255	279	260	-453	-544	-696

Table S5. Data collection and refinement statistics for metal-stripped Mn^{II} *Fj* β

	***Fj* β (aerobic)[1]**	***Fj* β (anaerobic)**
Data collection		
Space group	$P\,3_1$	$P\,3_1$
Cell dimensions		
a, *b*, *c* (Å)	53.69, 53.69, 221.84	53.45, 53.46, 220.75
α, β, γ (°)	90.0, 90.0, 120.0	90.0, 90.0, 120.0
Resolution (Å)	46.50-1.87 (1.90-1.87)*	46.29-1.92 (1.95-1.92)
R_{merge}	0.072 (0.939)	0.095 (0.927)
R_{pim}	0.030 (0.426)	0.040 (0.429)
$I / \sigma I$	24.3 (1.6)	18.3 (1.0)
$CC_{1/2}$	0.673	0.547
Completeness (%)	95.8 (54.5)	86.6 (35.7)
Redundancy	5.7 (4.7)	5.0 (3.7)
Refinement		
Resolution (Å)	46.50-1.87	46.29-1.92
No. reflections	59035	53967
R_{work} / R_{free}	0.207/0.233	0.206/0.245
No. atoms	5141	5106
Protein	5034	5034
Ligand/ion	6	4
Water	96	68
B-factors		
Protein	25.9	24.6
Ligand/ion	20.5	11.3
Water	20.6	17.5
r.m.s. deviations		
Bond lengths (Å)	0.0094	0.0098
Bond angles (°)	1.299	1.315
Molprobity clashscore	0.09 (100^{th} percentile)	2.81 (99^{th} percentile)
Rotamer outliers (%)	0.17	0
Ramachandran favored (%)	97.18	97.84
PDB accession code	6CWO	6CWP

[1]Two crystals were used to solve the structure. *Values in parentheses are for highest-resolution shell.

Table S6. Data collection and refinement statistics for as-isolated strep-tagged *Fj* β

	as-isolated *Fj* β native	**as-isolated *Fj* β** Mn anomalous
Data collection		
Space group	*P* 1	*P* 1
Cell dimensions		
a, *b*, *c* (Å)	48.36, 50.82, 79.29	48.36, 50.82, 79.29
α, β, γ (°)	106.2, 105.0, 95.8	106.2, 105.0, 95.8
Resolution (Å)	50.0-1.90 (1.93-1.90)*	50.0-2.95 (3.00-2.95)
R_{merge}	0.066 (0.592)	0.085 (0.417)
R_{pim}	0.035 (0.313)	0.052 (0.312)
$I / \sigma I$	15.8 (7.9)	12.8 (2.1)
$CC_{1/2}$	0.673	0.787
Completeness (%)	96.0 (94.9)	92.3 (71.7)
Redundancy	3.4 (3.3)	3.6 (2.2)
Refinement		
Resolution (Å)	50.0-1.90	
No. reflections	49275	
R_{work} / R_{free}	0.192/0.212	
No. atoms		
Protein	5068	
Ligand/ion	6	
Water	187	
B-factors		
Protein	23.2	
Ligand/ion	23.4	
Water	25.7	
r.m.s. deviations		
Bond lengths (Å)	0.006	
Bond angles (°)	0.9797	
Molprobity clashscore	1.89 (100^{th} percentile)	
Rotamer outliers (%)	1.3	
Ramachandran favored (%)	97.8	
PDB accession code	6CWQ	

*Values in parentheses are for highest-resolution shell.

Supporting References

[1] Jiang, W., Saleh, L., Barr, E. W., Xie, J., Gardner, M. M., Krebs, C., and Bollinger, J. M., Jr. (2008) Branched activation- and catalysis-specific pathways for electron relay to the manganese/iron cofactor in ribonucleotide reductase from *Chlamydia trachomatis*, *Biochemistry 47*, 8477-8484.

[2] Morán, J. F., James, E. K., Rubio, M. C., Sarath, G., Klucas, R. V., and Becana, M. (2003) Functional characterization and expression of a cytosolic iron-superoxide dismutase from cowpea root nodules, *Plant Physiol 133*, 773-782.

[3] McCord, J. M., and Fridovich, I. (1969) Superoxide dismutase. An enzymic function for erythrocuprein (hemocuprein), *J Biol Chem 244*, 6049-6055.

[4] Fish, W. W. (1988) Rapid colorimetric micromethod for the quantitation of complexed iron in biological samples, *Methods Enzymol 158*, 357-364.

[5] Zhang, Y., and Stubbe, J. (2011) *Bacillus subtilis* class Ib ribonucleotide reductase is a dimanganese(III)-tyrosyl radical enzyme, *Biochemistry 50*, 5615-5623.

[6] Long, F., Vagin, A. A., Young, P., and Murshudov, G. N. (2008) BALBES: a molecular-replacement pipeline, *Acta Crystallogr D 64*, 125-132.

[7] Stubbe, J., Nocera, D. G., Yee, C. S., and Chang, M. C. Y. (2003) Radical initiation in the class I ribonucleotide reductase: long-range proton-coupled electron transfer?, *Chem Rev 103*, 2167-2201.

[8] Ho, B. K., and Gruswitz, F. (2008) HOLLOW: generating accurate representations of channel and interior surfaces in molecular structures, *BMC Struct Biol 8*, 49.

[9] Volkamer, A., Kuhn, D., Rippmann, F., and Rarey, M. (2012) DoGSiteScorer: a web server for automatic binding site prediction, analysis and druggability assessment, *Bioinformatics 28*, 2074-2075.

[10] Gerlt, J. A., Bouvier, J. T., Davidson, D. B., Imker, H. J., Sadkhin, B., Slater, D. R., and Whalen, K. L. (2015) Enzyme Function Initiative-Enzyme Similarity Tool (EFI-EST): A web tool for generating protein sequence similarity networks, *Biochim Biophys Acta 1854*, 1019-1037.

[11] Jiang, W., Yun, D., Saleh, L., Barr, E. W., Xing, G., Hoffart, L. M., Maslak, M. A., Krebs, C., and Bollinger, J. M., Jr. (2007) A manganese(IV)/iron(III) cofactor in *Chlamydia trachomatis* ribonucleotide reductase, *Science 316*, 1188-1191.

[12] Landau, M., Mayrose, I., Rosenberg, Y., Glaser, F., Martz, E., Pupko, T., and Ben-Tal, N. (2005) ConSurf 2005: the projection of evolutionary conservation scores of residues on protein structures, *Nucleic Acids Research 33*, W299-W302.

[13] Cotruvo, J. A., Jr., Stich, T. A., Britt, R. D., and Stubbe, J. (2013) Mechanism of assembly of the dimanganese-tyrosyl radical cofactor of class Ib ribonucleotide reductase: Enzymatic generation of superoxide is required for tyrosine oxidation via a Mn(III)Mn(IV) intermediate, *J Am Chem Soc 135*, 4027-4039.

[14] Haddy, A., Waldo, G. S., Sands, R. H., and Penner-Hahn, J. E. (1994) Simulation of multifrequency EPR spectra from Mn(III)/Mn(IV) catalase of *Lactobacillus plantarum* using a new approach based on perturbation theory, *Inorg Chem 33*, 2677-2682.

[15] Zheng, M., Khangulov, S. V., Dismukes, G. C., and Barynin, V. V. (1994) Electronic structure of dimanganese(II,III) and dimanganese(III,IV) complexes and dimanganese catalase enzyme: a general EPR spectral simulation approach, *Inorg Chem 33*, 382-387.

[16] Teutloff, C., Schafer, K. O., Sinnecker, S., Barynin, V., Bittl, R., Wieghardt, K., Lendzian, F., and Lubitz, W. (2005) High-field EPR investigations of $Mn^{III}Mn^{IV}$ and $Mn^{II}Mn^{III}$ states of dimanganese catalase and related model systems, *Magn Reson Chem 43*, S51-S64.

[17] Cox, N., Ames, W., Epel, B., Kulik, L. V., Rapatskiy, L., Neese, F., Messinger, J., Wieghardt, K., and Lubitz, W. (2011) Electronic structure of a weakly antiferromagnetically coupled Mn(II)Mn(III) model relevant to manganese proteins: a combined EPR, ^{55}Mn-ENDOR, and DFT study, *Inorg Chem 50*, 8238-8251.